

1 ***Klebsiella pneumoniae* hijacks the Toll-IL-1R protein SARM1 in a type I IFN-dependent**
2 **manner to antagonize host immunity.**

3 Claudia Feriotti¹, Joana Sa-Pessoa¹, Ricardo Calderón-González¹, Lili Gu², Brenda Morris¹,
4 Ryoichi Sugisawa², Jose L. Insua¹, Michael Carty², Amy Dumigan¹, Rebecca J. Ingram¹, Adrien
5 Kisenpfening¹, Andrew G. Bowie², José A. Bengoechea^{1*}

6 ¹Wellcome-Wolfson Institute for Experimental Medicine. School of Medicine, Dentistry and
7 Biomedical Sciences, Queen's University Belfast, 97 Lisburn Road, Belfast

8 ²School of Biochemistry and Immunology, Trinity Biomedical Sciences Institute, Trinity College
9 Dublin, Dublin 2, Ireland

10

11 * Corresponding author: j.bengoechea@qub.ac.uk

12

13

14 The authors have declared that no conflict of interest exists.

15

16

17

18

19

20

21

22

23

24 **SUMMARY**

25 Many bacterial pathogens antagonize host defence responses by translocating effector proteins into
26 cells. It remains an open question how those pathogens not encoding effectors counteract anti-
27 bacterial immunity. Here, we show that *Klebsiella pneumoniae* hijacks the evolutionary conserved
28 innate immune protein SARM1 to control cell intrinsic immunity. *Klebsiella* exploits SARM1 to
29 regulate negatively MyD88 and TRIF-governed inflammation, and the activation of the MAP
30 kinases ERK and JNK. SARM1 is required for *Klebsiella* induction of IL10 by fine-tuning the p38-
31 type I IFN axis. SARM1 inhibits the activation of *Klebsiella*-induced absent in melanoma 2
32 inflammasome to limit IL1 β production, suppressing further inflammation. *Klebsiella* exploits type
33 I IFNs to induce SARM1 in a capsule and LPS O-polysaccharide-dependent manner via TLR4-
34 TRAM-TRIF-IRF3-IFNAR1 pathway. Absence of SARM1 reduces the intracellular survival of *K.*
35 *pneumoniae* in macrophages whereas *sarm1* deficient mice control the infection. Altogether, our
36 results illustrate a hitherto unknown anti-immunology strategy deployed by a human pathogen.

37

38

39

40

41

42

43

44

45

46

47 INTRODUCTION

48 *Klebsiella pneumoniae* is one of the pathogens sweeping the World in the antimicrobial
49 resistance pandemic. More than a third of the *K. pneumoniae* isolates reported to the European
50 Centre for Disease Prevention and Control were resistant to at least one antimicrobial group,
51 being the most common resistance phenotype the combined resistance to fluoroquinolones, third-
52 generation cephalosporins and aminoglycosides (Penalva et al., 2019). In addition, *Klebsiella*
53 species are a known reservoir for antibiotic resistant genes, which can spread to other Gram-
54 negative bacteria. Infections caused by multidrug resistant *K. pneumoniae* are associated with high
55 mortality rates and prolonged hospitalization (Giske et al., 2008). Alarmingly, recent studies have
56 also recognised that *K. pneumoniae* strains have access to a mobile pool of virulence genes (Holt et
57 al., 2015; Lam et al., 2018); enabling the emergence of a multidrug, hypervirulent *K. pneumoniae*
58 clone capable of causing untreatable infections in healthy individuals. Worryingly, there are already
59 reports describing the isolation of such strains (Gu et al., 2018; Yao et al., 2018; Zhang et al., 2015;
60 Zhang et al., 2016). Unfortunately, at present, we cannot identify candidate compounds in late-stage
61 development for treatment of multidrug *K. pneumoniae* infections. This pathogen is exemplary of
62 the mismatch between unmet medical needs and the current antimicrobial research and development
63 pipeline.

64 An attractive approach to develop new therapeutics against *K. pneumoniae* infections is to
65 boost innate immune defence mechanisms. Indeed, more than two decades of research demonstrates
66 the need of an adequate activation of the innate immune system for the clearance of *K. pneumoniae*
67 (Bengoechea and Sa Pessoa, 2019). However, this pathway requires an in-depth understanding of
68 which innate responses benefit the host versus the pathogen, as well as deconstructing the strategies
69 used by *K. pneumoniae* to survive within the infected tissue. In this regard, the fact that *K.*
70 *pneumoniae* does not encode type III or IV secretion systems known to deliver effectors into
71 immune cells, or any of the toxins affecting cell biology, makes interesting to uncover how the
72 pathogen controls the activation of immune cells.

73 Successful elimination of infections by the innate immune system is dependent on the
74 activation of pattern recognition receptors (PRRs) detecting the so-called pathogen-associated
75 molecular patterns (PAMPs). The PRRs Toll-like receptor (TLR) 4 and TLR2 play a significant role
76 restricting *K. pneumoniae* infection (Wieland et al., 2011). TLR4 and TLR2 signal via the adaptors
77 MyD88 and TRIF leading to the activation of NF- κ B and IRF3, respectively. These transcription
78 factors and MAP kinases control the activation of host defence antimicrobial responses (Jenner and
79 Young, 2005). The fact that *IL1R*^{-/-} mice are exquisitely susceptible to *K. pneumoniae* infection
80 demonstrates the importance of IL1 β -controlled responses for host survival and bacterial clearance
81 (Cai et al., 2012). Production of the mature active form of IL1 β requires the expression of the pro-
82 IL1 β , following PRR-mediated recognition of a pathogen, and its cleavage by caspase 1 to release
83 the active form of the cytokine. The activation of caspase 1 also leads to pyroptosis through the
84 proteolytic cleavage of gasdermin-D (GSDMD). The activation of caspase 1 requires the assembly
85 of a multiprotein platform, known as an inflammasome. Evidence suggests that *K. pneumoniae*
86 induces the secretion of IL1 β in vivo and in vitro via inflammasome activation (Cai et al., 2012;
87 Willingham et al., 2009b). Whether *K. pneumoniae* has evolved any strategy to limit early events of
88 TLR signalling, and inflammasome activation remains an open question.

89 SARM1 (Sterile α and HEAT Armadillo motif-containing protein) is an evolutionary
90 conserved innate immune protein across mammalian species with identities higher than 90%
91 (Belinda et al., 2008). Moreover, analysis of human SARM1 has revealed no nonsense mutations
92 and a worldwide selective sweep, indicating a strong selective pressure to preserve the integrity of
93 the protein (Fornarino et al., 2011). SARM1 contains a Toll-IL-1R (TIR) domain (Bratkowski et al.,
94 2020; O'Neill and Bowie, 2007). The presence of this domain indicates a role in IL1 and TLR
95 signalling. Interestingly, bacterial proteins containing the TIR domain interfere with TLR signalling
96 to inhibit innate immune responses (Askarian et al., 2014; Cirl et al., 2008; Coronas-Serna et al.,
97 2020; Imbert et al., 2017; Xiong et al., 2019). It is intriguing that the SARM1 TIR domain is more
98 closely related to bacteria TIR proteins than to the other mammalian TIR containing adaptors

99 (Zhang et al., 2011). Therefore, it can be speculated that SARM1 may play a negative role
100 regulating TLR signalling. Indeed, there is data suggesting that SARM1 inhibits lipopolysaccharide
101 (LPS)-induced signalling via TLR4-TRIF and TLR4-MyD88 pathways (Carlsson et al., 2016; Carty
102 et al., 2006). Furthermore, recent work has uncovered that SARM1 negatively regulates IL1 β
103 release by directly targeting the NLRP3 inflammasome (Carty et al., 2019). Collectively, this
104 evidence led us to speculate whether *K. pneumoniae* may hijack SARM1, an endogenous TIR-
105 containing protein regulating TLR and inflammasome activation, to control immune responses. The
106 role of SARM1 in infections has been only conclusively established to restrict West Nile virus
107 infection in the central nervous system (Szretter et al., 2009; Uccellini et al., 2020). *Sarm1*^{-/-} mice
108 do not control West Nile virus infection, and this is associated with enhanced mortality (Szretter et
109 al., 2009; Uccellini et al., 2020). To the best of our knowledge, there is no evidence supporting any
110 role of SARM1 in bacterial infections.

111 Here, we reveal that hypervirulent *K. pneumoniae* leverages the immunomodulatory roles of
112 SARM1 to control cell intrinsic immunity. We show that *K. pneumoniae* negatively regulates TLR-
113 governed inflammatory responses via SARM1. We demonstrate that SARM1 is required for *K.*
114 *pneumoniae*-induction of the anti-inflammatory cytokine IL10. We identify absent in melanoma 2
115 (AIM2) as the inflammasome activated by *K. pneumoniae* that is inhibited directly by SARM1 to
116 limit IL1 β production. We establish that *K. pneumoniae* exploits the immune effector type I IFNs to
117 induce SARM1 in a capsule and LPS O-polysaccharide-dependent manner. In vitro, absence of
118 SARM1 reduces the intracellular survival of *K. pneumoniae* in macrophages due to the recruitment
119 of lysosomes to the *Klebsiella* containing vacuole (KCV), whereas, in vivo, *Sarm1*^{-/-} mice clear the
120 infection. Collectively, our findings illustrate the crucial role of SARM1 in *K. pneumoniae* immune
121 evasion strategies, revealing one of the Achilles heel of our immune system exploited by the
122 pathogen to overcome host protective responses.

123 RESULTS

124 SARM1 negatively regulates *K. pneumoniae*-induced inflammation.

125 To examine the effect of SARM1 on *K. pneumoniae*-induced responses, we infected
126 immortalized bone marrow derived macrophages (iBMDMs) from wild-type and *sarm1*^{-/-} mice with
127 the hypervirulent strain of *K. pneumoniae* CIP52.145 (hereafter Kp52145). This strain belongs to
128 the *K. pneumoniae* KpI group and it encodes all virulence functions associated with invasive
129 community-acquired disease in humans (Holt et al., 2015; Lery et al., 2014). In the supernatants of
130 cells lacking SARM1, we observed a significant increase in the levels of the MyD88-dependent
131 cytokines TNF α , and IL1 β , and of the TRIF-dependent cytokines CXCL10 and type I IFNs
132 following Kp52145 infection. (Fig 1A). The levels of the TRIF-dependent proteins ISG15 and
133 Viperin were also higher in the lysates of Kp52145-infected *sarm1*^{-/-} macrophages than in those of
134 wild-type cells (Fig 1B). Kp52145 also increased the levels of the MyD88-dependent cytokines
135 TNF α , and IL1 β , and of the TRIF-dependent cytokine CXCL10 in BMDMs from *sarm1*^{-/-} mice (Fig
136 S1A), ruling out that the heightened responses observed in immortalized *sarm1*^{-/-} cells were due to
137 the process of immortalization of the cells. To confirm that the phenotype of *sarm1*^{-/-} cells was due
138 to the absence of the SARM protein, rescue experiments were performed by retroviral expression of
139 FLAG-SARM1 in *sarm1*^{-/-} iBMDMs. Following infection with Kp52145, we observed a reduction
140 in the levels of TNF α , IL1 β , and CXCL10 in FLAG SARM1 cells compare to those found in
141 infected *sarm1*^{-/-} macrophages (Fig 1C). Collectively, these data demonstrate that SARM1
142 negatively regulates *K. pneumoniae*-induced inflammation.

143 Recently, it has been reported that commercially available *sarm1*^{-/-} mice carry a passenger
144 mutation which may affect cytokine responses due to the background of the knockout strains and
145 not due to the absence of SARM1 protein (Uccellini et al., 2020). Although the cytokines affected
146 are not those assessed in our study, we decided to examine the role of SARM1 in *K. pneumoniae*
147 infection by reducing its levels via siRNA. Control experiments showed the reduction of the *Sarm1*
148 transcript in transfected iBMDMs with SARM siRNA (Fig S1B), confirming knockdown. We again
149 found higher levels of IL1 β , TNF α , and CXCL10 in the supernatants of infected *sarm1* knockdown
150 macrophages that in macrophages transfected with a non-targeting (All Stars) siRNA control (Fig

151 S1C). To provide additional support to our observations demonstrating a role of SARM1 as
152 negative regulator of *K. pneumoniae*-induced inflammation, we challenged iBMDMs from a
153 recently described new knockout SARM1 strain generated using CRISPR/Cas9-mediated genome
154 engineering, *Sarm1^{em1.ITft}* (Doran et al., 2021). Kp52145 induced a heightened inflammatory
155 response in *Sarm1^{em1.ITft}* macrophages compared to wild-type ones from littermates (Fig S1D).
156 Altogether, these data provide further evidence supporting the role of SARM1 to attenuate *K.*
157 *pneumoniae*-induced inflammation.

158 To determine whether the observed changes in cytokine production in the absence of
159 SARM1 involved changes in the transcription of genes, we assessed the transcription of MyD88
160 and TRIF-dependent cytokines by real time quantitative PCR (RT-qPCR). Figure 1D shows that
161 Kp52145 increased the transcription of the MyD88-governed cytokines *tnfa*, *illb*, and of the TRIF-
162 controlled cytokine *ifnb* in *sarm1^{-/-}* macrophages compare to wild-type ones. The transcription of
163 the interferon-stimulated genes (ISG) *isg15*, *mx1* and *ifit1* was also upregulated in infected *sarm1^{-/-}*
164 cells (Fig 1D).

165 The fact that the transcription factors NF- κ B and IRF3 governs the MyD88 and TRIF-
166 dependent responses, respectively led us to determine whether SARM1 regulates these pathways in
167 *K. pneumoniae*-infected cells. In the NF- κ B signalling cascade, the IKK α/β kinase controls the
168 phosphorylation of I κ B α that leads to the subsequent degradation of the protein by the ubiquitin
169 proteasome, allowing the nuclear translocation of NF- κ B (Taniguchi and Karin, 2018).
170 Immunoblotting analysis showed an increase in the phosphorylation of IKK α/β in *sarm1^{-/-}*
171 macrophages following infection (Fig 1E). As expected, we observed an increased phosphorylation
172 of I κ B α with a concomitant reduction in the levels of total I κ B α in Kp52145-infected *sarm1^{-/-}*
173 macrophages compare to wild-type ones (Fig 1E). Altogether, these results show an enhance
174 activation of NF- κ B in infected *sarm1^{-/-}* macrophages. To investigate the activation of the IRF3
175 signalling cascade, we assessed the phosphorylation of TBK1 and IRF3. TBK1 is the kinase
176 mediating the phosphorylation of IRF3 which it is an essential event for IRF3 nuclear translocation

177 (Fitzgerald et al., 2003). Immunoblotting experiments revealed an increased phosphorylation of
178 TBK1 and IRF3 in Kp52145-infected *sarm1*^{-/-} macrophages (Fig 1F), hence confirming an
179 increased activation of IRF3 in the absence of SARM1.

180 Reconstitution experiments in HEK293 cells by transfecting SARM1, and either MyD88 or
181 TRIF, and reporter systems to assess activation of NF-κB and IRF3 have demonstrated that SARM1
182 interacts with MyD88 and TRIF to block the activation of these signalling pathways (Carlsson et
183 al., 2016; Carty et al., 2006). Therefore, we sought to determine whether *K. pneumoniae* infection
184 would induce the interaction between SARM1, and MyD88, and TRIF. There is no commercially
185 available antibody to assess mouse SARM1 protein levels reliably. Therefore, to facilitate these
186 experiments, we took advantage of a recently described mouse expressing an epitope-tagged
187 SARM1 endogenously with a triple FLAG tag and double strep tag on the C-terminal end,
188 *Sarm1*^{FLAG} (Doran et al., 2021). Control experiments confirmed that the tagged protein retain
189 functionality (Doran et al., 2021). Figure 1G shows that in *Sarm1*^{FLAG} iBMDMs SARM1-FLAG co-
190 immunoprecipitates MyD88-HA and TRIF-HA only in Kp52145-infected cells, indicating that *K.*
191 *pneumoniae*-induced interaction of SARM1 with MyD88 and TRIF explains the reduced activation
192 of NF-κB and IRF3.

193 We next assessed the activation of MAPKs due to their role in governing the expression of
194 inflammatory genes (Dong et al., 2002). There is indirect evidence suggesting that SARM1 inhibits
195 MAPK activation (Peng et al., 2010). The activation of the three MAPKs p38, JNK and ERK
196 occurs through phosphorylation of serine and threonine residues. Western blot analysis showed an
197 increase in the levels of phosphorylated ERK and JNK in infected *sarm1*^{-/-} macrophages compared
198 to infected wild-type cells (Fig 1H). In contrast, there was a reduction in the phosphorylation of p38
199 in infected *sarm1*^{-/-} macrophages (Fig 1H). These results indicate that SARM1 exerts a negative
200 effect on the activation of ERK and JNK whereas SARM1 is needed for the activation of p38
201 following *K. pneumoniae* infection.

202 **SARM1 is required for *K. pneumoniae* induction of IL10 via p38.**

203 We next sought to determine the effect of the reduced activation of p38 in the absence of
204 SARM1 following *K. pneumoniae* infection. Because the activation of p38 is linked to the
205 production of IL10 (Saraiva and O'Garra, 2010), we asked whether SARM1 would affect *K.*
206 *pneumoniae* induction of IL10. Control experiments confirmed that the p38 inhibitor SB203580
207 abrogated Kp52145-induced production of IL10 in wild-type cells (Fig S2A), connecting p38
208 activation and IL10 production in *K. pneumoniae*-infected macrophages. Consistent with the
209 reduced activation of p38 in *sarm1*^{-/-} macrophages, RT-qPCR analysis showed a reduction in *il10*
210 transcription in the absence of SARM1 (Fig 2A). As expected, the levels of IL10 were significantly
211 lower in the supernatants of Kp52145-infected *sarm1*^{-/-} macrophages than in those from infected
212 wild-type cells (Fig 2B). The reduced levels of IL10 found in infected *sarm1*^{-/-} macrophages were
213 consistent with the reduced phosphorylation of the IL10-governed transcriptional factor STAT3 in
214 Kp52145-infected *sarm1*^{-/-} macrophages (Fig 2C). The addition of recombinant IL10 to Kp52145-
215 infected *sarm1*^{-/-} macrophages decreased the levels of IL1 β , TNF α , and CXCL10 (Fig 2D),
216 suggesting that the reduced levels of IL10 in the absence of SARM1 contributes to the upregulation
217 of inflammation in infected *sarm1*^{-/-} macrophages. Interestingly, Kp52145 did increase the levels of
218 *il1b*, *tnfa*, and *cxcl10* in *il10*^{-/-} *sarm1* knockdown macrophages beyond the levels found in *il10*^{-/-}
219 infected cells (Fig 2E), suggesting that the regulatory effect of SARM1 on inflammation is the sum
220 of the IL10-dependent attenuation, and the direct negative effect of SARM1 on MyD88 and TRIF
221 previously shown. The efficiency of *sarm1* knockdown in the *il10*^{-/-} background is shown in Figure
222 S2B.

223 To explain the reduced activation of p38 in the absence of SARM1, we reasoned that the
224 heightened inflammation upon infection of *sarm1*^{-/-} macrophages might have a negative effect on
225 p38 activation. Because there are reports demonstrating a connection between type I IFN signalling
226 and p38 (Ivashkiv and Donlin, 2014), we speculated that the elevated levels of type I IFNs found in
227 Kp52145-infected *sarm1*^{-/-} macrophages might underline the reduced activation of p38. To explore

228 this possibility, we asked whether abrogating type I IFN signalling in the absence of SARM1 could
229 rescue p38 activation following infection. Indeed, when the infection of *sarm1*^{-/-} macrophages was
230 done in the presence of blocking antibodies against the type I IFN receptor (IFNAR1) we observed
231 an increase in the levels of phosphorylated p38 (Fig 2F). Likewise, we observed an increase in the
232 levels of phosphorylated p38 in infected wild-type cells treated with the IFNAR1 receptor blocking
233 antibody (Fig 2G), reinforcing the connection between type I IFN levels and *K. pneumoniae*-
234 induced activation of p38. As anticipated, the levels of IL10 were higher in cells treated with the
235 IFNAR1 blocking antibody than in those treated with the isotype control antibody (Fig 2H). In turn,
236 we found a reduction in the levels of IL1 β , and TNF α in the supernatants of cells treated with the
237 blocking antibody (Fig 2I). The connection between type I IFN and p38 activation in *K.*
238 *pneumoniae*-infected macrophages was further corroborated by the fact that Kp52145-induced p38
239 phosphorylation was higher in *ifnar1*^{-/-} cells than in wild-type ones (Fig S2C). Likewise, we found
240 an increase phosphorylation of p38 in infected *tlr4*^{-/-} (Fig S2D), and *tram*^{-/-}*trif*^{-/-} macrophages (Fig
241 S2E), which is consistent with the fact that TLR4-TRAM-TRIF signalling mediates the production
242 of *K. pneumoniae*-induced type I IFN (Ivin et al., 2017). As we anticipated, the levels of *il10* were
243 higher in infected *tlr4*^{-/-}, *tram*^{-/-}*trif*^{-/-} and *ifnar1*^{-/-} macrophages compare to infected wild-type cells
244 (Fig S2F).

245 Altogether, these data demonstrate that absence of SARM1 impairs *K. pneumoniae*-
246 mediated activation of p38 due to the negative regulation exerted by type I IFN. The reduced
247 activation of p38 limits the levels of IL10 induced by *K. pneumoniae* with a concomitant increase in
248 inflammation.

249 **SARM1 negatively regulates *K. pneumoniae*-induced AIM2 inflammasome activation.**

250 The increased production of IL1 β by *K. pneumoniae*-infected *sarm1*^{-/-} macrophages led us to
251 characterize the effect of SARM1 on *K. pneumoniae*-triggered inflammasome activation.
252 Immunoblotting experiments showed elevated levels of cleavage of pro-IL1 β (Fig 3A), and an

253 increased activation of caspase 1 in infected *sarm1*^{-/-} macrophages compared to infected wild-type
254 cells (Fig 3B). Absence of SARM1 resulted in enhanced levels of processed GSDMD following
255 infection (Fig 3C). The use of the caspase 1 inhibitor YVAD (Motani et al., 2011) confirmed that
256 the release of IL1 β by Kp52145-infected wild-type and *sarm1*^{-/-} macrophages was caspase 1-
257 dependent (Fig 3D). Additional experiments supported that the adaptor protein ASC and GSDMD
258 are required for IL1 β release after inflammasome activation in *Klebsiella*-infected cells because we
259 found a significant decrease levels of IL1 β in the supernatants of infected *asc*^{-/-} and *gsdmd*^{-/-}
260 macrophages compared to infected wild-type cells (Fig S3A). Moreover, immunoblotting
261 experiments showed a decrease in the levels of processed pro-IL1 β in the supernatants of infected
262 *asc*^{-/-} and *gsdmd*^{-/-} macrophages (Fig S3B). Together, these results are consistent with enhanced
263 inflammasome activation in *K. pneumoniae*-infected *sarm1*^{-/-} macrophages. To sustain this notion
264 further, we examined whether absence of SARM1 affects ASC speck formation. After
265 inflammasome activation, ASC oligomerizes in large protein aggregates enabling the subsequent of
266 clustering of caspase 1 (Cai et al., 2014; Lu et al., 2014). Therefore, detection of ASC specks is a
267 distinguish feature of inflammasome activation. Single cell analysis by flow cytometry revealed that
268 a greater percentage of cells displayed ASC-speck formation after Kp52145 infection of *sarm1*^{-/-}
269 macrophages (Fig 3E). Collectively, these results show that SARM1 negatively regulates
270 inflammasome activation following *K. pneumoniae* infection.

271 We next sought to identify the inflammasome regulated by SARM1 in Kp52145-infected
272 cells. Because SARM1 has been shown to inhibit NLRP3 (Carty et al., 2019), we asked whether
273 NLRP3 mediates the secretion of IL1 β following *K. pneumoniae* infection. However, Figure S3C
274 shows that the NLRP3 inhibitor MCC950 (Coll et al., 2015) did not reduce Kp52145-induced
275 secretion of IL1 β . Furthermore, we found no reduction in IL1 β levels in the supernatants of infected
276 *nlrp3*^{-/-} macrophages compared to wild-type cells (Fig S3D), and no decrease in the levels of
277 cleavage pro-IL1 β (Fig S3E). Control experiments showed that Kp52145 infection even increased
278 the levels of NLRP3 (Fig S3F). Altogether, these data demonstrates that NLRP3 is not required for

279 *K. pneumoniae* induction of IL1 β . Although NLRC4 mediates IL1 β secretion following infection
280 with other Gram-negative pathogens, we consider unlikely that *K. pneumoniae* activates NLRC4
281 because *Klebsiella* does not express any of the bacterial proteins known to activate this
282 inflammasome. We next considered whether AIM2, which it is also activated by Gram-negative
283 pathogens (Ge et al., 2012; Rathinam et al., 2010; Tsuchiya et al., 2010), might mediate *K.*
284 *pneumoniae*-induced release of IL1 β . Indeed, IL1 β release was abrogated in Kp52145-infected
285 *aim2*^{-/-} macrophages (Fig 3F). Further corroborating that AIM2 is the inflammasome activated by *K.*
286 *pneumoniae*, neither caspase 1 nor GSDMD were processed in infected *aim2*^{-/-} macrophages (Fig
287 3G). Moreover, ASC-speck formation was not detected in infected *aim2*^{-/-} cells in contrast to
288 infected wild type and *nlrp3*^{-/-} cells (Fig 3E). The fact that the percentage of cells with ASC-specks
289 was not significantly different between wild type and *nlrp3*^{-/-} macrophages corroborates further that
290 *K. pneumoniae* does not activate the NLRP3 inflammasome. Collectively, this evidence
291 demonstrates that AIM2 is the inflammasome mediating IL1 β release following *K. pneumoniae*
292 infection. However, the possibility exists that other inflammasome(s) might be activated in the
293 absence of SARM1. To confirm that indeed AIM2 mediates IL1 β secretion in Kp52145-infected
294 *sarm1*^{-/-} macrophages, we reduced *aim2* levels by siRNA in *sarm1*^{-/-} macrophages. Control
295 experiments confirmed the knockdown efficiency (Fig S3F). As we expected, we found a reduction
296 in IL1 β levels in the supernatants of *aim2* knockdown cells compared to All stars siRNA transfected
297 control cells (Fig 3H). Treatment of infected *sarm1*^{-/-} macrophages with the NLRP3 inhibitor
298 MCC950 did not result in any decrease in IL1 β levels (Fig 3H), indicating that *K. pneumoniae* does
299 not activate NLRP3 even in the absence of SARM1.

300 To examine whether SARM1 had a direct effect on AIM2, we reconstituted the AIM2
301 inflammasome in HEK293 cells by transfecting plasmids expressing pro-IL-1 β , pro-caspase-1,
302 ASC, and AIM2. Under these conditions, the inflammasome is active to induce the secretion of
303 IL1 β without external stimulus (Shi et al., 2016), and this is AIM2-dependent since no detectable
304 mature IL-1 β was produced from cells transfected with all the inflammasome components except

305 AIM2 (Fig 3I). AIM2-dependent secretion of IL1 β was inhibited by the expression of SARM1 (Fig
306 3I). We next determined which domains of SARM1 were required for AIM2 inhibition by
307 expressing different truncations of SARM1. This experiment showed that the TIR domain alone
308 was sufficient to inhibit IL1 β release (Fig 3I). These data led us to determine whether *K.*
309 *pneumoniae* induces the interaction between SARM1 and AIM2 to inhibit inflammasome
310 activation. We carried out co-immunoprecipitation experiments infecting retrovirally transfected
311 FLAG-SARM1 in *sarm1*^{-/-} macrophages. Figure 3J shows that SARM1 immunoprecipitated AIM2
312 only in Kp52145-infected cells.

313 Altogether, we propose that *K. pneumoniae* exploits SARM1 to inhibit AIM2
314 inflammasome activation by a direct interaction between SARM1 and AIM2.

315 ***K. pneumoniae* induces AIM2 in a type I IFN-dependent manner.**

316 We next sought to investigate whether *K. pneumoniae* infection affects the expression levels
317 of AIM2. RT-qPCR analysis revealed that Kp52145 induced the expression of *aim2* in vitro (Fig
318 4A), and in the lungs of infected mice (Fig 4B). Western blot experiments demonstrated that
319 Kp52145 increased the expression of AIM2 in wild-type macrophages (Fig 4C). We next
320 investigated the signalling pathways governing *K. pneumoniae* induction of *aim2*. *Aim2* has been
321 identified as an ISG (Fernandes-Alnemri et al., 2009), and the interferome prediction tool (Rusinova
322 et al., 2013) indicates that type I IFN activates the expression of *aim2* in human and mouse cells.
323 Consistent with this prediction, *aim2* and AIM2 levels were reduced in *Klebsiella* infected *ifnar1*^{-/-}
324 cells (Fig 4D). We then tested whether *K. pneumoniae* would induce *aim2* and AIM2 in cells
325 deficient for the TLR4-TRAM-TRIF-IRF3 pathway mediating type I IFN production by *K.*
326 *pneumoniae* (Ivin et al., 2017). Indeed, Kp52145 did not increase *aim2* levels in *tlr4*^{-/-}, *tram*^{-/-}*trif*^{-/-}
327 and *irf3*^{-/-} macrophages (Fig S4A). No significant differences were found between infected wild-
328 type and *myd88*^{-/-} macrophages (Fig S4A). Kp52145 did not increase AIM2 levels in *tlr4*^{-/-}, and
329 *tram*^{-/-}*trif*^{-/-} macrophages (Fig S4B). Together, these results demonstrate that *K. pneumoniae*

330 infection induces AIM2 in a type I IFN-dependent manner following activation of TLR4-TRAM-
331 TRIF-IRF3 pathway. These results led us to investigate whether the capsule polysaccharide (CPS),
332 and LPS O-polysaccharide, mediating the production of type I IFN following *K. pneumoniae*
333 infection (Ivin et al., 2017), are involved in *aim2* induction. Cells were infected with single mutants
334 lacking each of the polysaccharides, and a double mutant lacking both (Ivin et al., 2017; Sa-Pessoa
335 et al., 2020). Indeed, the three mutants induced less *aim2* than the wild-type strain (Fig 4E).
336 Furthermore, immunoblotting analysis showed that the three mutants did not increase AIM2 levels
337 (Fig 4F). As anticipated, the CPS and LPS O-polysaccharide mutants induced less IL1 β than the
338 wild-type strain, being the double mutant the strain inducing the lowest IL1 β levels (Fig 4G).

339 To further link type I IFN signalling to *K. pneumoniae*-induced AIM2 inflammasome
340 activation, we determined IL1 β production in cells deficient for the signalling pathway mediating
341 type I IFN production following *K. pneumoniae* infection. As expected, Kp52145 did not induce the
342 release of IL1 β in *tlr4*^{-/-}, *tram*^{-/-}*trif*^{-/-} and *ifnar1*^{-/-} macrophages (Fig S4C). Control experiments
343 showed that pro-IL β production was not significantly reduced in infected *tlr4*^{-/-} cells, ruling out that
344 the lack of IL1 β production in the absence of TLR4 was due to reduced levels of pro-IL1 β (Fig
345 S4D).

346 Collectively, these results demonstrate that signalling via IFNAR1 is required for activation
347 of AIM2 inflammasome by *K. pneumoniae* upon recognition of the CPS and the LPS O-
348 polysaccharide by TLR4.

349 ***K. pneumoniae* induces SARM1 in a type I IFN-dependent manner.**

350 It is common for pathogens to upregulate or activate the expression of the host proteins they
351 do target for their own benefit. It might be then expected that *K. pneumoniae* upregulates the
352 expression of SARM1. Indeed, Kp52145 induced the expression of *sarm1* in vitro (Fig 5A), and in
353 the lungs of infected mice (Fig 5B). Infection of *Sarm1*^{FLAG} cells confirmed that Kp52145 increased
354 the expression of SARM1 (Fig 5C). We next sought to identify the signalling pathways governing

355 *K. pneumoniae* induction of *sarm1*; however, the regulation of SARM1 is poorly understood.
356 Analysis of the promoter region of SARM1 interrogating the interferome database (Rusinova et al.,
357 2013) identified SARM1 as an ISG. Therefore, we speculated that *K. pneumoniae* may regulate
358 SARM1 in a type I IFN-dependent manner. Providing initial support to this notion, RT-qPCR
359 analysis showed that Kp52145 did not induce *sarm1* in *ifnar1*^{-/-} macrophages (Fig 5C).
360 Furthermore, *sarm1* levels were reduced in infected *tlr4*^{-/-}, *tram*^{-/-}*trif*^{-/-}, and *irf3*^{-/-} macrophages (Fig
361 5C). As anticipated, Kp52145 induced *sarm1* in *myd88*^{-/-} macrophages (Fig 5C). These results led
362 us to investigate whether the CPS, and the LPS O-polysaccharide are involved in *sarm1* induction.
363 Indeed, the three mutants induced less *sarm1* than the wild-type strain, although the double mutant
364 lacking CPS and the LPS O-polysaccharide induced less *sarm1* than each of the single mutants did
365 (Fig 5D).

366 Altogether, these results confirm experimentally that *K. pneumoniae* leverages type I IFN
367 signalling to induce SARM1 following activation of TLR4-TRAM-TRIF-IRF3 pathway. The CPS
368 and the LPS O-polysaccharide are the *K. pneumoniae* factors responsible for the upregulation of the
369 expression of SARM1.

370 **SARM1 promotes *K. pneumoniae* virulence.**

371 Having established that *K. pneumoniae* exploits the immunomodulatory roles of SARM1 to
372 control MyD88 and TRIF-governed cytokine production, and the activation of AIM2
373 inflammasome, we next sought to investigate whether SARM1 contributes to *K. pneumoniae*
374 subversion of cell-autonomous immunity. We have demonstrated that *K. pneumoniae* manipulates
375 the phagosome traffic following phagocytosis to create a unique niche that does not fuse with
376 lysosomes, the KCV, allowing the intracellular survival of *Klebsiella* (Cano et al., 2015). Therefore,
377 we asked whether the absence of SARM1 impairs *K. pneumoniae* intracellular survival. Control
378 experiments revealed that the attachment of Kp52145 was not affected in *sarm1*^{-/-} cells (Fig S5A)
379 whereas there was a slight reduction in the number of engulfed bacteria (Fig S5B). Time-course

380 experiments revealed that the intracellular survival of Kp52145 was significantly reduced in *sarm1*^{-/-}
381 macrophages (Fig 6A). We then sought to determine whether the reduced intracellular survival
382 was due to an increase in the colocalization of lysosomes with the KCV. Lysosomes were labelled
383 with the membrane-permeant fluorophore cresyl violet (Ostrowski et al., 2016), and cells were
384 infected with GFP-labelled Kp52145 to assess the KCV at the single cell level by
385 immunofluorescence. Confocal microscopy experiments revealed that the majority of the KCVs
386 from wild-type macrophages did not colocalize with cresyl violet (Fig 6B and Fig 6C),
387 corroborating our previous work (Cano et al., 2015). In contrast, there was an increase in the
388 colocalization of KCVs from *sarm1*^{-/-} macrophages with cresyl violet (Fig 6B and Fig 6C),
389 demonstrating that the absence of SARM1 results in the fusion of the KCV with lysosomes with a
390 concomitant reduction in the numbers of intracellular bacteria.

391 Previously, we showed that *K. pneumoniae* targets the PI3K-AKT axis to survive
392 intracellularly (Cano et al., 2015). Therefore, we asked whether the absence of SARM1 would
393 affect *K. pneumoniae*-induced AKT phosphorylation. Immunoblotting experiments confirmed that
394 Kp52145-induced phosphorylation of AKT was reduced in *sarm1*^{-/-} macrophages compare to wild-
395 type cells (Fig 6D). In *K. pneumoniae*-infected cells, AKT activation is linked to the recruitment of
396 Rab14 to the KCV to block the fusion with lysosomes (Cano et al., 2015). We then investigated the
397 recruitment of Rab14 to the KCV in *sarm1*^{-/-} macrophages. Figure 6E illustrates that Rab14 does not
398 colocalize with the KCV in *sarm1*^{-/-} macrophages in contrast to wild-type macrophages. Altogether,
399 this evidence demonstrates that SARM1 is crucial for *K. pneumoniae*-induced activation of the
400 PI3K–AKT–Rab14 axis to control the phagosome maturation to survive inside macrophages.

401 To obtain a global view of the role of SARM1 in *K. pneumoniae* infection biology, we
402 examined the contribution of SARM1 to modulate the inflammatory responses induced by *K.*
403 *pneumoniae* in vivo. We analysed several inflammatory-associated cytokines and chemokines in the
404 lungs of *K. pneumoniae*-infected animals. Kp52145 induced the expression of *il1b*, *tnfa*, *il12*,
405 *cxcl10* *ifnb*, and *isg15* in vivo (Fig 7A), although the levels of *il1b*, *tnfa*, and *il12* were significantly

406 higher in *sarm1*^{-/-} mice than in wild-type ones. Furthermore, we observed a significant decrease in
407 the levels of *il10* in *sarm1*^{-/-} mice compare to wild-type ones (Fig 7B). Similar results were obtained
408 infecting *Sarm1*^{em1.1Tft} mice, indicating that the results are neither dependent on the mouse strain nor
409 on the way the *sarm1* knock-out mice were generated (Fig 7A and Fig 7B). Together, these results
410 demonstrate that the absence of SARM1 in vivo results in heightened inflammation following *K.*
411 *pneumoniae* infection.

412 To find out whether the absence of SARM1 has any effect on immune cells, we used mass
413 cytometry to profile the cells of infected and non-infected mice. We tested a panel of 33 surface and
414 intracellular markers that would enable resolution of 100 lymphoid and myeloid cell types (Table
415 S1). To define cell communities, we employed the clustering algorithm PhenoGraph (Levine et al.,
416 2015). In *sarm1*^{-/-} non-infected mice, we found a significant increase in the numbers of resident
417 monocytes (MHC-II-Ly6G-Ly6C⁺CD11b⁺CD11c-CCR2^{high}) ($p < 0.05$) compare to non-infected
418 wild-type mice, whereas there were no significant differences in the numbers of any other immune
419 cell (Fig 7C). Following infection, we observed a significant increase in the numbers of neutrophils
420 (MHC-II⁺Ly6G⁺Ly6C⁺F4/80^{-low}) in both genotypes, although the numbers were not significantly
421 different between them (Fig 7C). In infected wild-type mice there was an increase in the numbers of
422 interstitial macrophages (MHC-II⁺Ly6G⁺Ly6C⁺CD11b⁺) compared to infected *sarm1*^{-/-} mice ($p <$
423 0.01) (Fig 7C). In contrast, there was a significant increase in the number of alveolar macrophages
424 (MHC-II⁺Ly6G⁻Ly6C⁻CD11b^{low}CD11c⁺) ($p < 0.01$) in infected *sarm1*^{-/-} mice compared to infected
425 wild-type ones (Fig 7C). The numbers of alveolar macrophages were not significantly different
426 between infected and non-infected *sarm1*^{-/-} mice. There were no significant differences in the
427 numbers of other immune cells between infected genotypes (Fig 7C).

428 PhenoGraph analysis identified 30 clusters with similar marker expression (Fig S6A and
429 Table S2). The heat map of the markers expressed by each of the clusters is shown in Figure S6B.
430 Differences were found between samples (Fig 7D, and Fig S6C). Clusters 11 and 12 were only
431 present in *sarm1*^{-/-} infected mice whereas clusters 13 and 15 were only present in wild-type-infected

432 mice. These four clusters represent different subsets of neutrophils (Fig S6A). Heat map analysis of
433 these clusters revealed that in both genetic backgrounds each of the clusters can be differentiated
434 based on the expression levels of PD-L1 and CD86 (Fig 7E). Clusters 11 and 12 were characterized
435 by the expression levels of the markers Ly6C, CD11b, CD24, IL10, Siglec H and LAP-TGF β (Fig
436 7B), revealing an increase activation of neutrophils in *sarm1*^{-/-} mice following infection. Clusters 5
437 and 6, corresponding to alveolar macrophages (Fig S6A), were predominant in *sarm1*^{-/-} mice, and
438 they can be differentiated by the expression of CCR2. The expression of CCR2 is higher in cluster 6
439 than in cluster 5. No major differences were noted between genetic backgrounds with infection,
440 except that *sarm1*^{-/-} cells showed an increase in the levels of IL10 (p <0.0001) (Fig 7H). Differences
441 were found between the subsets of interstitial macrophages. Cluster 16 was the predominant in
442 wild-type infected mice, whereas cluster 17 was the predominant one in *sarm1*^{-/-} infected mice (Fig
443 7D). The levels of CD11c differentiates both clusters, higher in cluster 17 than in cluster 16 (Fig
444 7G). High levels of CD11c are associated with the activation of immune cells (Arnold et al., 2016;
445 Lewis et al., 2015). Cells belonging to cluster 17, found in *sarm1*^{-/-} mice, were characterized by
446 high levels of CD11b, iNOS, Ly6C, CCR2, Siglec H, SIRP α , LAP-TGF β , CD44, CD86. MHC-II,
447 and Cd11c (Fig 7G), all markers of activation of immune cells. Altogether, mass cytometry analysis
448 demonstrate an increase in the numbers of neutrophils and alveolar macrophages in *sarm1*^{-/-}
449 infected mice. These cells are crucial in host defence against *K. pneumoniae* (Broug-Holub et al.,
450 1997; Xiong et al., 2015; Xiong et al., 2016; Ye et al., 2001). Furthermore, PhenoGraph cluster
451 analysis revealed the presence of different subsets of neutrophils and interstitial macrophages in
452 *sarm1*^{-/-} infected mice characterized by elevated levels of markers associated with the activation of
453 immune cells.

454 Finally, we determined the ability of *sarm1*^{-/-} mice to control bacterial growth following
455 intranasal infection. At 24 h post infection, there was a 94% reduction in bacterial load in the lungs
456 of infected *sarm1*^{-/-} mice compared to wild-type infected ones (Fig 7H). Moreover, we found a
457 significant lower dissemination of Kp52145 to liver and spleen in *sarm1*^{-/-} mice than in wild-type

458 ones (Fig 7I). The infection of *Sarm1*^{em1.1Tjt} mice yielded similar results; the knockout mice
459 controlled the lung infection more efficiently than the wild-type ones and there was less
460 dissemination to deeper tissues (Fig 7H and Fig 7I). Altogether, this evidence establishes the
461 crucial role of SARM1 for *K. pneumoniae* survival in vivo.

462

463 DISCUSSION

464 The human pathogen *K. pneumoniae* exemplifies the global threat of antibiotic resistant
465 bacteria. Hundreds of mobile antimicrobial resistant genes are found in *K. pneumoniae*, and these
466 can be disseminated to other bacteria. *K. pneumoniae* is the species within which several new
467 antimicrobial resistance genes were first discovered (e.g. carbapenem-resistance genes KPC, OXA-
468 48 and NDM-1). Less obvious, but central to pathogenesis, are *K. pneumoniae* adaptations to the
469 human immune system allowing the pathogen to flourish in the tissues. However, our knowledge of
470 the strategies deployed by *K. pneumoniae* to counteract the innate immune system is still
471 elementary, as it is our understanding of which of such responses benefit the host versus *K.*
472 *pneumoniae*. In this study, we show that *K. pneumoniae* exploits SARM1 to control MyD88 and
473 TRIF-governed inflammation, to limit the activation of the MAP kinases ERK and JNK, and to
474 induce the anti-inflammatory cytokine IL10 by fine-tuning the p38-type I IFN axis. SARM1 also
475 inhibits the activation of *K. pneumoniae*-induced AIM2 inflammasome with a concomitant
476 reduction in IL1 β (Fig 8) to further suppress inflammatory responses. We have established that
477 SARM1 is necessary for *K. pneumoniae* intracellular survival whereas, in vivo, absence of SARM1
478 facilitates the clearance of the pathogen. Altogether, these results demonstrate that SARM1 plays an
479 integral role in *K. pneumoniae* infection biology. Manipulation of the Toll-IL-1R protein SARM1 is
480 a hitherto unknown anti-immunology strategy deployed by a human pathogen.

481 The evidence of this study suggests that *K. pneumoniae* leverages the TIR-TIR interactions
482 between SARM1, and MyD88 and TRIF to attenuate MyD88 and TRIF-dependent inflammatory

483 responses. There are few examples of pathogens exploiting TIR-TIR interactions to blunt the
484 activation of TLR-controlled signalling pathways (Askarian et al., 2014; Cirl et al., 2008; Coronas-
485 Serna et al., 2020; Imbert et al., 2017; Xiong et al., 2019). However, and without exception, these
486 pathogens deploy a prokaryotic protein containing the TIR domain into immune cells, whereas *K.*
487 *pneumoniae* is the first pathogen hijacking an endogenous mammalian TIR-containing protein.
488 SARM1TIR domain is more closely related to bacteria TIR proteins than to the other mammalian
489 TIR containing adaptors (Zhang et al., 2011). This data highlights an evolutionary convergence
490 between *K. pneumoniae* and the pathogens encoding TIR containing proteins to exploit TIR-TIR
491 interactions to attenuate inflammation.

492 Another novel finding of our work is that the absence of SARM1 impairs *K. pneumoniae*
493 induction of IL10. IL10 production complements the reduction in inflammation achieved by
494 limiting the activation of TLR signalling due to TIR-TIR interactions following the recognition of
495 *K. pneumoniae* by PRRs. The fact that neutralization of the cytokine enhances the clearance of the
496 pathogen (Greenberger et al., 1995) illustrates the crucial role of IL10 in *K. pneumoniae* infection
497 biology. How *K. pneumoniae* induces IL10 was unknown. Our data implicates p38 whose
498 activation is fine-tuned by type I IFN elicited by *K. pneumoniae*. The absence of SARM1 perturbs
499 the p38-type I IFN axis by increasing the levels of type I IFN, resulting in a reduction of *K.*
500 *pneumoniae*-induced p38 activation with a concomitant reduction in the production of IL10. The
501 regulatory connection between type I IFNs and IL10 has been described; however, and in contrast
502 to our results, the data indicates that type I IFN signalling is needed to sustain IL10 production in
503 macrophages following challenge with LPS or *Mycobacterium spp.* (Chang et al., 2007; McNab et
504 al., 2014; Pattison et al., 2012). These results reflect the importance of type I IFNs levels in the
505 host-pathogen interface although the consequences are context dependent.

506 Previous work has demonstrated the importance of IL1 β -governed responses in host defence
507 against *K. pneumoniae* (Cai et al., 2012). Not surprisingly, *K. pneumoniae* has evolved to blunt
508 IL1 β -mediated inflammation (Frank et al., 2013; Regueiro et al., 2011). However, there was no

509 evidence indicating whether *K. pneumoniae* is able to counteract inflammasome activation to limit
510 the production of IL1 β . Here we demonstrate that SARM1 inhibits inflammasome activation by *K.*
511 *pneumoniae*. The fact that SARM1 has recently been shown to inhibit NLRP3 activation (Carty et
512 al., 2019), and that there are observations indicating that *K. pneumoniae* may activate NLRP3
513 inflammasome (Hua et al., 2015; Willingham et al., 2009a), made plausible that SARM1 would
514 inhibit NLRP3 activation in *K. pneumoniae* infected cells. However, this was not the case. Our data
515 demonstrate that AIM2 is the inflammasome activated by *K. pneumoniae* that it is inhibited by
516 SARM1. Components of the type I IFN signalling pathway were essential for the activation of
517 AIM2 inflammasome by *K. pneumoniae*. This is similar to *Listeria monocytogenes* and *Francisella*
518 *spp*, two other pathogens activating AIM2 (Fernandes-Alnemri et al., 2010; Henry et al., 2007;
519 Jones et al., 2010; Man et al., 2015; Rathinam et al., 2010; Tsuchiya et al., 2010), reinforcing the
520 link between type I IFN signalling and AIM2 inflammasome. However, cGAS-STING-IRF3-
521 IFNAR1 signalling is necessary in the case of *Listeria* and *Francisella*-mediated activation of
522 AIM2 (Fernandes-Alnemri et al., 2010; Hansen et al., 2014; Man et al., 2015; Rathinam et al.,
523 2010), whereas TLR4-TRAM-TRIF-IRF3-IFNAR1 mediates *K. pneumoniae* induction of AIM2.
524 This evidence uncovers the crucial role of IRF3-IFNAR1 signalling in the host-bacteria interface.
525 Recently, we have demonstrated the importance of this hub to control *K. pneumoniae* infections
526 (Ivin et al., 2017).

527 Mechanistically, *K. pneumoniae* triggered an association between SARM1 and AIM2, and
528 the SARM1 TIR domain was sufficient to inhibit AIM2 activation. Altogether, our data is
529 consistent with a model in which SARM1 directly targets AIM2 to suppress the recruitment of ASC
530 and ASC-speck formation, restraining the activation of caspase 1. To the best of our knowledge, *K.*
531 *pneumoniae* is the first pathogen deploying a strategy to target directly AIM2 activation because the
532 other known examples are based on reducing the activating signal (Ge et al., 2012; Ulland et al.,
533 2010). On the other hand, the strategy deployed by *K. pneumoniae* is reminiscent of how cells avoid

534 an excessive activation of AIM2 by leveraging two small proteins, p202 in mouse, and IFI16 β in
535 human cells, that impede AIM2-ASC complex formation (Wang et al., 2018; Yin et al., 2013).

536 It is intriguing that *K. pneumoniae* did not activate NLRP3 even in the background of
537 *sarm1*^{-/-} and *aim2*^{-/-} cells. This is even more puzzling considering that *K. pneumoniae* increased the
538 expression of NLRP3. Considering that the stimuli reported to activate NLRP3, such as ROS, are
539 most likely also present in *K. pneumoniae*-infected cells, it is then tempting to speculate that *K.*
540 *pneumoniae* has evolved mechanisms to blunt the activation of NLRP3. Future studies are
541 warranted to uncover how *K. pneumoniae* inhibits NLRP3 activation.

542 Except in neurons, the levels of SARM1 are low in most cells types, including monocytes
543 and macrophages (Doran et al., 2021; Uhlen et al., 2010), suggesting that SARM1 levels are under
544 tight control. We provide evidence demonstrating that *K. pneumoniae* induced SARM1 in a type I
545 IFN dependent manner via a TLR4-TRAM-TRIF-IRF3-IFNAR1 signalling pathway, hence placing
546 SARM1 as an ISG. Likewise SARM1, type I IFNs are also conserved during evolution and appear
547 in the first vertebrates (Secombes and Zou, 2017), suggesting that *K. pneumoniae* manipulates an
548 ancient SARM1-type I IFNs axis to counteract the activation of host defences. It is interesting to
549 note the complex interface between *K. pneumoniae* and type I IFN. On the one hand, TRIF-
550 mediated type I IFN is essential for host defence against *K. pneumoniae* (Cai et al., 2009; Ivin et al.,
551 2017) including the expression of IL1 β as a result of AIM2 activation (this work), and to limit the
552 production of IL10 (this work). On the other hand, *K. pneumoniae* exploits type I IFN to induce
553 SARM1 to attenuate TRIF and AIM2 activation. This evidence supports the notion that there is a
554 threshold of type I IFN levels that needs to be reached in order to exert a protective role whereas
555 below this threshold type I IFNs promote *K. pneumoniae* infection. In this scenario, SARM1 is one
556 of the breaks that *K. pneumoniae* uses to control type I IFNs. Future studies should investigate
557 whether *K. pneumoniae* uses other means to control the levels of type I IFNs.

558 We were keen to identify the bacterial factor(s) mediating the expression of SARM1. *K.*
559 *pneumoniae* does not encode any type III or IV secretion system or any of the toxins implicated in
560 counteracting innate immunity, making then interesting to uncover how *K. pneumoniae* manipulates
561 any host protein. Our results establish that the CPS and the LPS O-polysaccharide induced the
562 expression of SARM1. This is in perfect agreement with the evidence demonstrating that both
563 polysaccharides trigger the production of type I IFNs (Ivin et al., 2017). Importantly, these
564 polysaccharides are required for *K. pneumoniae* survival in mice (pneumonia model) (Cortes et al.,
565 2002; Lawlor et al., 2005; Tomas et al., 2015), underlining the importance of SARM1 induction as
566 a *K. pneumoniae* virulence trait since this process is abrogated in these mutant strains. We recently
567 demonstrated that both polysaccharides are crucial to reduce the SUMOylation of proteins to limit
568 host defence responses involving type I IFN-regulated miRNAs of the *let-7* family (Sa-Pessoa et al.,
569 2020). Altogether, this evidence underscores the role of *K. pneumoniae* CPS and LPS to hijack
570 regulators of the host immune system, hence expanding their well-established role in *K.*
571 *pneumoniae* stealth behaviour (Bengoechea and Sa Pessoa, 2019).

572 Previous work established that *K. pneumoniae* survives intracellularly in macrophages
573 residing in the KCV (Cano et al., 2015). Here, we demonstrate that SARM1 is essential for the
574 survival of *K. pneumoniae*. Mechanistically, absence of SARM1 impaired *K. pneumoniae*-induced
575 activation of AKT which in turn limited the recruitment of Rab14 to the KCV resulting in the fusion
576 of the KCV with lysosomes ((Cano et al., 2015) and this work). The reduction in AKT activation
577 found in *sarm1*^{-/-} cells also explains the reduction of phagocytosis of *K. pneumoniae* because
578 previous studies have demonstrated conclusively the connection between PI3-K-AKT activation
579 and phagocytosis of bacteria, including *K. pneumoniae*, and large particles (Cano et al., 2015;
580 Schlam et al., 2015). It is intriguing to note that two other pathogens, *Salmonella typhimurium* and
581 *M. tuberculosis*, also manipulate the PI3K-AKT-Rab14 pathway to arrest phagosome maturation
582 (Kuijl et al., 2007; Kyei et al., 2006). It is then tempting to postulate that SARM1 may also play an
583 important role in the intracellular survival of these two pathogens. If this is the case, the axis

584 SARM1-PI3K-AKT-Rab14 will become one of the central nodes targeted by pathogens to take
585 control over cellular functions. Current efforts of the laboratory are devoted to investigate this
586 hypothesis.

587 The fact that *sarm1* deficient mice were more efficient at controlling *K. pneumoniae*
588 infection than wild-type mice provides strong support to the notion that *K. pneumoniae* leverages
589 SARM1 to counteract host defences. Somewhat unexpectedly considering our in vitro results, we
590 found a reduction in the levels of type I IFN and ISGs in infected *sarm1* deficient mice. This might
591 be due to the fact that type I IFNs and ISGs are produced early during *K. pneumoniae* infection
592 (Ivin et al., 2017). Nonetheless, it is important to realize that type I IFN signalling is essential to
593 control *K. pneumoniae* infections (Ivin et al., 2017). On the other hand, the in vivo data support that
594 *K. pneumoniae* exploits SARM1 to limit inflammatory cytokines and chemokines, and to produce
595 IL10, mirroring the in vitro results. Interestingly, a wealth of evidence supports that this type of
596 lung inflammatory environment is essential to clear *K. pneumoniae* infections (Bengoechea and Sa
597 Pessoa, 2019). Therefore, it can be concluded that *K. pneumoniae* exploits SARM1 to modify the
598 lung microenvironment to flourish. Mass cytometry analysis uncovered the presence of high
599 numbers of alveolar macrophages, and neutrophils in *sarm1*^{-/-} deficient mice. This is in good
600 agreement with previous studies showing the importance of these cell types for the clearance of *K.*
601 *pneumoniae* infections (Broug-Holub et al., 1997; Xiong et al., 2015; Xiong et al., 2016). Our
602 profile analysis revealed subsets of neutrophils and interstitial macrophages only present in *sarm1*^{-/-}
603 infected mice. These cells expressed high levels of markers associated with immune activation
604 further reinforcing the notion that the microenvironment in the absence of SARM1 supports *K.*
605 *pneumoniae* clearance.

606 *K. pneumoniae* nosocomial infections are associated with high morbidity and mortality
607 (Giske et al., 2008), and, worryingly, there is an increase in the number of community acquired
608 infections (Lipworth et al., 2021; Magiorakos et al., 2013). Not surprisingly, the World Health
609 Organization has singled out *K. pneumoniae* as a global threat to human health, and includes the

610 pathogen among those for which new therapeutics are urgently needed. Our findings, including in
611 vivo experiments probing a pre-clinical pneumonia mouse model, provide compelling evidence
612 demonstrating that SARM1 is a target to boost human defence mechanisms against *K. pneumoniae*.
613 Host-directed therapeutics aiming to interfere with host factors required by pathogens to counter the
614 immune system are emerging as untapped opportunities that are urgently needed in the face of the
615 global pandemic of antibiotic resistant infections. SARM1 is a druggable protein, and the crystal
616 structure of the TIR domain of SARM1 is solved at 1.8 Å (Horsefield et al., 2019). This high-
617 resolution structural information should facilitate the development of small-molecule inhibitors.
618 Indeed, major efforts are underway to develop pharmacological approaches to inhibit SARM1 in the
619 context of diseases with pathophysiological neuronal cell death (DiAntonio, 2019; Hughes et al.,
620 2021). Based on the results of this study, we propose that these drugs shall show a beneficial effect
621 to treat *K. pneumoniae* infections alone or as a synergistic add-on to antibiotic treatment. Future
622 studies shall confirm whether this is the case.

623

624 **MATERIALS and METHODS**

625 **Ethics statement**

626 The experiments involving mice were approved by the Queen's University Belfast's Ethics
627 Committee and conducted in accordance with the UK Home Office regulations (project licences
628 PPL2778 and PPL2910) issued by the UK Home Office. Animals were randomized for
629 interventions but researches processing the samples and analysing the data were aware which
630 intervention group corresponded to which cohort of animals.

631 **Bacterial strains and growth conditions**

632 Kp52145 is a clinical isolate (serotype O1:K2) previously described (Lery et al., 2014; Nassif et al.,
633 1989). The *cps* mutant strain, 52145- Δ *manC*, the mutant lacking the LPS O-polysaccharide, 52145-

634 Δglf , and the double mutant lacking the CPS and the LPS O-polysaccharide, 52145- Δwca_{k2} - Δglf ,
635 are isogenic strains of Kp52145 and they have been described previously (Kidd et al., 2017; Sa-
636 Pessoa et al., 2020). Strain 52145- Δglf expresses similar levels of CPS than the wild-type strain (Sa-
637 Pessoa et al., 2020). Bacteria were grown in 5 ml Luria-Bertani (LB) medium at 37 °C on an orbital
638 shaker (180 rpm), and where appropriate, antibiotics were added to the growth medium at the
639 following concentration: carbenicillin, 50 µg/ml; chloramphenicol, 25 µg/ml.

640 **Mammalian cells and cell culture.**

641 iBMDMs cells from wild-type (WT), $tlr4^{-/-}$, $myd88^{-/-}$, and $tram^{-/-}trif^{-/-}$ mice on a C57BL/6
642 background were obtained from BEI Resources (NIAID, NIH) (repository numbers NR-9456, NR-
643 9458, NR-15633, and NR-9568, respectively). $Il-10^{-/-}$ and $irf3^{-/-}$ iBMDMs were described
644 previously (Bartholomew et al., 2019; Ivin et al., 2017). Additional iBMDMs were generated as
645 previously described (Sa-Pessoa et al., 2020). Briefly, tibias and femurs from C57BL/6, $ifnar1^{-/-}$,
646 $sarm1^{-/-}$, $Sarm1^{em1.ITf}$, $Sarm1^{FLAG}$, $aim2^{-/-}$, $nlrp3^{-/-}$, $casp-1^{-/-}$, $asc^{-/-}$, and $gsdmd^{-/-}$ were removed using
647 sterile techniques, and the bone marrow was flushed with fresh medium. To obtain macrophages,
648 cells were plated in Dulbecco's modified Eagle's medium (DMEM) supplemented with 20%
649 filtered L929 cell supernatant (a source of macrophage colony-stimulating factor) and maintained at
650 37°C in a humidified atmosphere of 5% CO₂. Medium was replaced with fresh supplemental
651 medium after 1 day. Immortalization of BMDMs was performed after 5 days by exposing them for
652 24 h to the J2 CRE virus (carrying v-myc and v-Raf/v-Mil oncogenes, kindly donated by Avinash
653 R. Shenoy, Imperial College London). This step was repeated 2□ days later (day 7), followed by
654 continuous culture in DMEM supplemented with 20% (vol/vol) filtered L929 cell supernatant for 4
655 to 6□ weeks. The presence of a homogeneous population of macrophages was accessed by flow
656 cytometry using antibodies for CD11b (clone M1/70; catalog number 17-0112-82; eBioscience) and
657 CD11c (clone N418; catalog number 48-0114-82; eBioscience). Retroviral transduction of SARM1
658 in $sarm1^{-/-}$ cells was done as previously described (Carty et al., 2006; Carty et al., 2019).

659 iBMDMs and BMDMs were grown in DMEM (catalog number 41965; Gibco) supplemented with
660 heat-inactivated fetal calf serum, 100 U/ml penicillin, and 0.1 mg/ml streptomycin (Gibco) at 37°C
661 in a humidified 5% CO₂ incubator. Cells were routinely tested for *Mycoplasma* contamination.
662 Cells were seeded a density of 2 x10⁴ cells/well in 24-well plates, 5 x10⁵ cells/well in 12-well
663 plates, and 2 x10⁶ cells/well in 6-well plates.

664 **Infection conditions.**

665 Overnight bacterial cultures were refreshed 1/10 into a new tube containing 4.5 mL of fresh LB.
666 After 2.5 h at 37°C, bacteria were pelleted (2500× g, 20 min, 22°C), resuspended in PBS and
667 adjusted to an optical density of 1.0 at 600 nm (5 x 10⁸ CFU/ml). Infections were performed using a
668 multiplicity of infection (MOI) of 100 bacteria per cell in a 1 ml volume. Synchronization of the
669 infection was performed by centrifugation (200 x g for 5 min). For incubation times longer than 30
670 min, cells were washed and 1 ml of fresh medium containing gentamycin (100 µg/ml) was added to
671 the wells to kill extracellular bacteria. Medium containing gentamycin was kept until the end of the
672 experiment. Infections were performed one day after seeding the cells in the same medium used to
673 maintain the cell line without antibiotics. Infected cells were incubated at 37°C in a humidified 5%
674 CO₂ incubator.

675 **siRNA experiments.**

676 For transfection of siRNAs, 2x10⁴ iBMDMs (6-well plates) were transfected in suspension with 20
677 nM siRNA using Lipofectamine RNAiMAX (Invitrogen) in 200 µl Opti-MEM I
678 (ThermoFisher). AllStars negative-control siRNA (Qiagen) or ON-TARGET plus SMART pool
679 siRNA targeting AIM2 (no. L-044968-01-0020; Dharmacon) and SARM1 (no. L-041633-01-0005;
680 Dharmacon) were used to transfect cells. The macrophages were infected 16 h post transfection.
681 Efficiency of transfection was confirmed by RT-qPCR analysis of duplicate samples from three
682 independent transfections by normalizing to the hypoxanthine phosphoribosyltransferase 1 (*hprt*)

683 gene and comparing gene expression in the knockdown sample with the AllStars negative control.

684 Primers are listed in Table S3.

685 **Inhibitors, recombinant cytokines, and blocking antibodies.**

686 The NLRP3 inhibitor MCC950 ([vehicle solution DMSO], 10 μ M CAS 256373-96-3 – Calbiochem,
687 Sigma), and the caspase 1 inhibitor YVAD ([vehicle solution DMSO], 10 μ M CAS 256373-96
688 Sigma) were added 2 h before infection to the cells. Recombinant mouse IL-10 ([vehicle solution
689 water] 1ng/ml, Biolegend) was added overnight before infection. The p38 inhibitor SB203580
690 ([vehicle solution DMSO], 10 μ M, Sigma) was added 2 h before infection. The mouse anti-IFNAR1
691 receptor antibody (clone MAR1-5A3 [vehicle solution water] 5 ng/ml, BioXcell) was added
692 overnight before infection. All these reagents were kept for the duration of the experiment.

693 **RNA isolation and RT-qPCR**

694 Infections were performed in 6-well plates. Cells were washed three times with pre-warmed sterile
695 PBS, and total RNA was extracted from the cells in 1 ml of TRIzol reagent (Ambion) according to
696 the manufacturer's instructions. Extracted RNA was treated with DNase I (Roche) and precipitated
697 with sodium acetate (Ambion) and ethanol. RNA was quantified using a Nanovue Plus
698 spectrophotometer (GE Healthcare Life Sciences). cDNA was generated by retrotranscription of 1g
699 of total RNA using M-MLV reverse transcriptase (Invitrogen) and random primers (Invitrogen).
700 Two duplicates were generated from each sample. Ten nanograms of cDNA were used as a
701 template in a 5- l reaction mixture from a KAPA SYBR FAST qPCR kit (Kapa Biosystems).
702 Primers used are listed in table S3. RT-qPCR was performed using a Rotor-Gene Q (Qiagen) with
703 the following thermocycling conditions: 95°C for 3 min for hot-start polymerase activation,
704 followed by 40 cycles of 95°C for 5 s and 60°C for 20 s. Fluorescence of SYBR green dye was
705 measured at 510 nm. Relative quantities of mRNAs were obtained using the $\Delta\Delta C_T$ method by using
706 hypoxanthine phosphoribosyltransferase 1 (*hprt*) gene normalization.

707 **Immunoblots**

708 Macrophages were seeded in 6-well plates for 24 h before infection. Cell lysates were prepared in
709 lysis buffer (1x SDS Sample Buffer, 62.5 mM Tris-HCl pH 6.8, 2% w/v SDS, 10% glycerol, 50
710 mM DTT, 0.01% w/v bromophenol blue). Proteins were resolved on 8, 10 or 12% SDS-PAGE gels
711 and electroblotted onto nitrocellulose membranes. Membranes were blocked with 3% (wt/vol)
712 bovine serum albumin in TBS-Tween (TBST), and specific antibodies were used to detect protein
713 using chemiluminescence reagents and a G:BOX Chemi XRQ chemiluminescence imager
714 (Syngene).

715 The following antibodies were used: anti-IL-1 β (anti-goat, 1:1000; # AF-401-NA, R&D Systems),
716 anti-caspase-1 (anti-rabbit, 1:1000; #24232, Cell Signaling), anti-AIM2 (anti-rabbit, 1:1000; sc-
717 515895, Santa Cruz), anti-NLRP3 (anti-mouse, 1:1000; #15101, Cell Signaling), anti-Gasdermin-D
718 (anti-rabbit, 1:1000; #93709, Cell Signaling), anti-Viperin (anti-rabbit, 1:1000 # NBP2-03971,
719 Novus Biologicals), anti-ISG15 (1:1000; #9636, Cell Signaling), anti-phospho-STAT3 (anti-rabbit,
720 1:1,000; #9145, Cell Signaling), anti-I κ B α (anti-rabbit, 1:1,000; #4814, Cell Signaling), anti-
721 phospho-I κ B α (Ser32) (anti-goat, 1:1,000; #9246, Cell Signaling), anti-phospho-AKT1/2/3 (Ser
722 473) (anti-rabbit, 1:1000; sc-33437, Santa Cruz), anti-phospho-IKK α/β (Ser176/180)(16A6) (anti-
723 rabbit, 1:1000; #2697, Cell Signaling), anti-phospho-IRF3 (Ser 396) (anti-rabbit, 1:1000; #4947,
724 Cell Signaling), anti-phospho-p-TBK-1/NAK (Ser172) (D52C2) (anti-rabbit, 1:1000; #5483, Cell
725 Signaling), anti-phospho-JNK (anti-rabbit, 1:1000; #9251S, Cell Signaling), anti-phospho-ERK
726 (anti-rabbit, 1:1000; #9101, Cell Signaling), anti-phospho-p38 MAPK (Thr180/Tyr182) (D3F9)
727 (anti-rabbit, 1:1000; #4511, Cell Signaling), anti-SARM1 (anti-chicken, 1:70; generated by
728 Icosagen by immunizing chicken with the TIR domain of human SARM1), anti-Flag M2 (1 μ g,
729 Sigma F3165), anti-HA (1:1000, Santa Cruz Biotechnology sc-805). Immunoreactive bands were
730 visualized by incubation with HRP-conjugated IgG Secondary antibody (anti-goat, 1:5000; #
731 HAF017, R&D Systems, goat anti-rabbit, 1:5000; #170-6515, Bio Rad, goat anti-mouse, 1:5000;
732 #6516, Bio-Rad). To ensure that equal amounts of proteins were loaded, blots were re-probed with
733 α -tubulin (1:3000; #T9026, Sigma- Aldrich) or β -actin (anti-mouse, 1:1000; sc-130065, Santa

734 Cruz). To detect multiple proteins, membranes were re-probed after stripping of previously used
735 antibodies using a pH 2.2 glycine-HCl/SDS buffer.

736 **Processing cell free supernatants for inflammasome studies**

737 iBMDMs were seeded in 6 wells plates and were infected 24 h later . At the indicated time points,
738 the plates were centrifuged at 200xg for 5 min. at room temperature, and the supernatants were
739 transferred to microcentrifuge tubes and placed on ice. The cells were lysed in 80 μ l of Laemmli
740 buffer with β -mercaptoethanol (1 in 19 ratio), collected in a microcentrifuge tube and stored at -
741 20°C. The supernatants were processed by adding 9 μ l of StrataClean Resin, hydroxylated silica
742 particles (Cat. 400714) per 1 ml of supernatant. The samples were homogenized in vortex for 1 min,
743 and were centrifuged at 9000 x g for 2 min. The supernatant was discarded, and the pellets were
744 suspended in 40 μ l of Laemmli buffer and transferred to filtered columns within collection tubes.
745 The columns were centrifuged at 8,000 x g at RT for 1 min, and the eluate collected. The samples
746 were boiled for 5 min in heat block at 95°C and loaded for western blot analysis.

747 **Enzyme-linked immunosorbent assay (ELISA), and cytokine measurement**

748 Infections were performed in 12-well plates. Supernatants from infected cells were collected at the
749 indicated time points in the figure legends, and spun down at 12,000 x g for 5 min to remove any
750 debris. TNF- α (#900-K54), IL-1 β (#900-K47), IL-10 (#900-K53) and IP-10 (CXCL10) (#250-16)
751 in the supernatants were quantified using ABTS ELISA Development Kit (PeproTech) according to
752 the manufacturer's instructions. All experiments were performed in duplicate, and three
753 independent experiments were conducted.

754 For quantification of type I IFN (INF- α/β) in the supernatants of iBMDMs, cells were infected for
755 16 h, and supernatants were collected. Murine type I IFNs were detected using B16-Blue IFN- α/β -
756 reporter cells (Invivogen) which carry an SEAP reporter gene under the control of the IFN- α/β -
757 inducible ISG54 promoter and that have an inactivation of the IFN- γ receptor. Supernatants from
758 iBMDM cells were incubated with the reporter cell line, and levels of SEAP in the supernatants

759 were determined using the detection medium QUANTI-Blue (Invivogen) after 24 h as per the
760 manufacturer's instructions using recombinant mouse IFN- β (PBL Assay Science, catalogue
761 number 12401-1) as a standard. Experiments were run in duplicates and repeated at least three
762 times. Results are expressed as OD at 655 nm.

763 **Detection of ASC specks formation by flow cytometry**

764 To detect ASC speck formation by flow cytometry, we adapted the protocol described by Sester and
765 colleagues (Sester et al., 2015). Cells were harvested from 6-wells plates with ice-cold PBS,
766 centrifuged at 1,000 x g for 5 min, and resuspended in 1 ml ice-cold PBS. Samples were then fixed
767 by the drop wise addition of 4 ml ice-cold molecular grade ethanol while vortexing. After 15 min,
768 cells were pelleted by centrifugation at 600 x g for 10 min, supernatants gently removed and pellets
769 suspended in 250 μ l ASC speck buffer (ASB, PBS/0.1% sodium azide, 0.1% BSA, 1.5% FCS)
770 containing 1 μ l Fc block anti-CD16/CD32 (2.4G2, BD Biosciences) for 20 min. To stain ASC
771 specks, 0.2 μ l anti-ASC (Cat# sc-22514R, Santa Cruz) in 50 μ l ASB buffer were added to the
772 samples, and incubated for 90 min at room temperature. The cells were washed with 1 ml ASB, and
773 the re suspended in 50 μ l ASB containing 0.1 μ l Alexa 488 goat anti-rabbit IgG (H+L) (Molecular
774 Probes). After 45 min, cells were washed with 1 ml ASB, and re suspended in 500 μ l ASB. Samples
775 were processed on a BD FACS Canto and analyzed using FlowJo X (Tree Star) software and
776 graphical representation.

777 **AIM2 reconstitution in HEK cells**

778 HEK293T cells were seeded at 2×10^5 cells/well in 24-well plates and incubated overnight. The cells
779 were transfected using Lipofectamine 2000 with plasmids expressing pro-IL-1 β -FLAG (50 ng), pro-
780 Caspase-1-FLAG (10 ng), ASC-FLAG (1 ng), HA-AIM2 (50 ng) and 10, 50 or 100 ng of
781 pdlNotInPkmCSR FLAG SARM1, FLAG SARM1 TIR, FLAG SARM1 Δ TIR or
782 pdlNotInPkmCSR empty vector control. Medium was replaced 24 h after transfection and
783 supernatants were collected 16 h after media change. Quantification of secreted murine IL-1 β was

784 performed using ELISA (R&D). Cells were lysed with RIPA buffer and subjected to
785 immunoblotting by using anti-HA or anti-FLAG antibodies for the detection of AIM2 and
786 SARM/SARM TIR/ SARM Δ TIR expression.

787 **Coimmunoprecipitation analysis**

788 iBMDMs were seeded onto 6-wells plates (8×10^5 cells/well). Cells were transfected the following
789 day with 1 μ g of MyD88-HA or TRIF-HA plasmids (Carty et al, 2006) diluted in 200 μ l of opti-
790 MEM (Gibco) using 6 μ l of Lipofectamine 2000 (Invitrogen). Transfected cells were infected 20 h
791 post transfection at a MOI of 100. After 1 h of contact, media was replaced by media containing
792 gentamicin (100 μ g/ml), and cells were collected at 3 h and lysed in RIPA buffer containing: 50
793 mM Tris-HCl, pH 7.2, 0.15 M NaCl, 0.1% SDS, 1% Sodium Deoxycholate, 1% Triton X-100 and
794 proteinase inhibitors: 1 mM PMSF and halt protease inhibitor cocktail (ThermoFisher Scientific,
795 catalogue number 78430). The whole cell lysates were centrifuged at 10,000 \times g for 20 minutes at 4
796 $^{\circ}$ C. The supernatants were transferred to a new tube and the pellets were kept to probe the input.
797 Whole cell lysates were incubated with 1 μ g FLAG (Sigma, F3165) or normal mouse IgG (Santa
798 Cruz, c-2025) antibodies for 2 hours at 4 $^{\circ}$ C in a rotary wheel mixer. Protein A/G Plus agarose
799 suspension (Santa Cruz # sc-2003) was added to the whole cells lysates suspension and incubated at
800 4 $^{\circ}$ C on a rotary mixer overnight. The suspension was centrifuged at 1,000 \times g for 4 min at 4 $^{\circ}$ C and
801 the supernatant was aspirated and discarded. Pellets were washed 2 times with RIPA buffer,
802 suspended in 40 μ l of 2 x electrophoresis sample buffer (Laemmli buffer) and boiled for 5 min at 95
803 $^{\circ}$ C.

804 **Adhesion, phagocytosis and intracellular survival**

805 iBMDMs were seeded in 12-well plates approximately 16 h before infection. Infections were
806 performed as previously described. To enumerate the number of bacteria adhered to macrophages,
807 after 30 min of contact cells were washed twice with PBS, and they were lysed in 300 μ l of 0.1%
808 (wt/vol) saponin in PBS for 5 min at 37 $^{\circ}$ C. Serial dilutions were plated in LB and the following day

809 bacterial CFUs were counted. Results are expressed as CFU per ml. To determine the number of
810 bacteria phagocytosed by the cells, after 30 min of contact, cells were washed once with PBS and
811 fresh medium containing gentamycin (100 µg/ml) was added to the wells. After 30 min, cells were
812 washed three times with PBS, and lysed with saponin. Samples were serially diluted in PBS and
813 plated in PBS. After 24 h incubation at 37°C, CFUs were counted and results expressed as CFUs
814 per ml. To assess intracellular survival, 4 h after the addition of gentamycin, cells were washed
815 three times with PBS and lysed with saponin. Serial dilutions were plated on LB to quantify the
816 number of intracellular bacteria. Results are expressed as % of survival (CFUs at 4 h versus 1 h in
817 *sarm1*^{-/-} cells normalized to the results obtained in wild-type macrophages set to 100%). All
818 experiments were carried out with triplicate samples on at least five independent occasions.

819 **Assessment of the colocalization of the KCV with cellular markers**

820 The protocol was adapted from (Cano et al., 2015). Briefly, wild-type and *sarm1*^{-/-} iBMDMs
821 (2x10⁴ per well) were grown on 13 mm circular coverslips in 24-well plates and were infected with
822 Kp52145 harbouring pFPV25.1Cm (March et al., 2013). After 30 min of contact the coverslips
823 were washed with PBS and gentamycin (100µg/ml in DMEM medium) was added to kill
824 extracellular bacteria.

825 **(i) Staining of lysosomes.**

826 Cresyl violet acetate salt (Sigma) was used to label lysosomes (Ostrowski et al., 2016). Cresyl
827 violet in fresh medium (5µM) was added to the cells 12 min before fixing the cells. The residual
828 fluid marker was removed by washing the cells three times with PBS, followed by fixation (4%
829 paraformaldehyde in PBS pH 7.4 for 20 min at room temperature). Coverslips were mounted
830 with ProLong™ Gold antifade mountant (Invitrogen). Coverslips were visualised on the Leica SP8
831 Confocal microscope within 24 h after fixing. To determine the percentage of bacteria that
832 co-localized with cresyl violet, bacteria located inside a minimum of 100 infected cells were

833 analysed in each experiment. Experiments were carried out in duplicate in three independent
834 occasions.

835 **(ii) Rab14 staining.**

836 At the indicated time points post infection, coverslips were washed with PBS and permeabilized
837 with 0.1% (w/v) saponin (Sigma) in PBS for 30 minutes. Coverslips were then incubated for 120
838 minutes with anti-Rab14 (4 µg/ml in 0.1% (v/v) horse serum (Gibco), 0.1% (w/v) saponin in PBS;
839 clone D-5, murine IgG1, sc-271401, Santa Cruz Biotechnologies), washed with PBS, followed by a
840 45 minutes incubation with anti-mouse IgG H&L labelled with AlexaFluor 647 (10 µg/ml in 0.1%
841 (v/v) horse serum (Gibco), 0.1% (w/v) saponin in PBS, polyclonal, donkey IgG, ab150111,
842 Abcam). Coverslips were washed with PBS, and then incubated with anti-Lamp1 (1 µg/ml in 0.1%
843 (v/v) horse serum (Gibco), 0.1% (w/v) saponin in PBS, clone 1D4B, rat IgG2a, sc-19992, Santa
844 Cruz Biotechnologies) for 20 min, washed with PBS, and incubated for 20 minutes with anti-rat
845 IgG H&L labelled with AlexaFluor 568 (10 µg/ml in 0.1% (v/v) horse serum (Gibco), 0.1% (w/v)
846 saponin in PBS, polyclonal, goat IgG, A11077, Life Technologies). Coverslips were mounted in
847 microscope slides with ProLong Gold antifade mountant (Invitrogen), and visualised on a TCS-SP5
848 inverted microscope (Leica Biosystems). To determine the percentage of the Lamp1 positive KCV
849 that co-localized with Rab14, KCVs of at least 100 infected cells from three independent
850 experiments were analysed.

851 **Intranasal murine infection model**

852 Infections were performed as previously described (Ivin et al., 2017). Briefly, 8- to 12-week-old
853 C57BL/6 mice (Charles River), *sarm1*^{-/-}, B6.129X1-Sarm1tm1Aidi/J (The Jackson Laboratory, and
854 bred at Queen's University Belfast), *Sarm1*^{em1.1Tjfl} (Doran et al., 2021) of both sexes were infected
855 intranasally with $\sim 3 \times 10^5$ Kp52145 in 30 µl PBS. Non-infected mice were mock infected with 30
856 µl sterile PBS. The number of mice per group are indicated in the figure legends. 24 h post
857 infection, mice were euthanized using a Schedule 1 method according to UK Home Office

858 approved protocols. For those mice used for mass cytometry analysis, 16 hours post infection, they
859 were dosed intraperitoneally with 500 µg of monensin (Sigma) for intracellular cytokine staining.

860 Left lung samples from infected and uninfected control mice were immersed in 1 ml of RNA
861 stabilisation solution (50% [w/v] ammonium sulphate, 2.9% [v/v] 0.5M ethylenediaminetetraacetic
862 acid, 1.8% [v/v] 1 M sodium citrate) on ice and then stored at 4°C for at least 24 h prior to RNA
863 extraction. Samples were homogenized in 1 ml ice-cold TRIzol (Ambion) using a VDI 12 tissue
864 homogenizer (VWR). RNA was extracted according to the manufacturer's instructions extraction,
865 and cDNA was generated by retrotranscription of 1 µg of total RNA using M-MLV reverse
866 transcriptase (Invitrogen) and random primers (Invitrogen). RT-qPCR analysis was undertaken
867 using the KAPA SYBR FAST qPCR Kit, oligonucleotide primers as described in the in vitro
868 protocol, and Rotor-Gene Q (Qiagen). Thermal cycling conditions were as follows: 95°C for 3 min
869 for enzyme activation, 40 cycles of denaturation at 95°C for 10 s and annealing at 60°C for 20 s.
870 Each cDNA sample was tested in duplicate, and relative mRNA quantity was determined by the
871 comparative threshold cycle ($\Delta\Delta C_T$) method using hypoxanthine phosphoribosyltransferase 1
872 (*mhprt*) gene normalisation.

873 Right lung, spleen and liver samples from infected mice were immersed in 1 ml sterile PBS on ice
874 and processed for quantitative bacterial culture immediately. Samples were homogenised with a
875 Precellys Evolution tissue homogenizer (Bertin Instruments), using 1.4 mm ceramic (zirconium
876 oxide) beads at 4500 rpm for 7 cycles of 10 seconds, with a 10-second pause between each cycle.
877 Homogenates were serially diluted in sterile PBS and plated onto *Salmonella-Shigella* agar (Sigma),
878 and the colonies were enumerated after overnight incubation at 37°C. Data were expressed as CFUs
879 per gr of tissue.

880 **Mass cytometry**

881 **(i) Generation of metal-labelled antibodies**

882 Carrier protein and glycerol-free antibodies were labelled with lanthanide isotopes using Maxpar
883 X8 Antibody Labelling Kits (Fluidigm) according to the manufacturer's instructions. Briefly, X8
884 polymer was loaded with the lanthanide isotope in L-buffer, and the metal-loaded polymer purified
885 and washed in C-buffer using an Amicon Ultra-0.5 centrifugal filter unit with 3kDa cutoff
886 (Millipore-Sigma). At the same time, the antibody was reduced with 4 mM tris(2-
887 carboxyethyl)phosphine hydrochloride (TCEP) solution in R-buffer, and purified in C-buffer, using
888 an Amicon Ultra-0.5 centrifugal filter unit with 50kDa cut-off (Millipore-Sigma).

889 Both the lanthanide-loaded polymer and the partially reduced antibody were mixed and incubated at
890 37 °C for 90 minutes. Once the incubation was completed, the conjugated antibody was washed
891 several times with W-buffer using an Amicon Ultra-0.5 centrifugal filter unit with 50kDa cut-off
892 (Millipore-Sigma), and quantified using a NanoDrop spectrophotometer (280 nm). The antibody
893 was finally resuspended in antibody stabilizer PBS supplemented with 0.05% sodium azide at a
894 final concentration of 0.5 mg/mL and stored at 4 °C.

895 **(ii) Mass cytometry staining and acquisition**

896 Mice lungs were aseptically collected in PBS and homogenized with a handheld homogenizer.
897 Single-cell suspensions were obtained by flushing the samples through 70 µM strainer, incubated
898 with nuclease (Pierce). Red blood cells were lysed with ACK buffer, and samples stained,
899 according to manufacturer's instructions. Briefly, cell suspensions were first incubated with 1 µM
900 of 103Rh for live/dead discrimination, and later with cell surface metal-labelled antibodies,
901 prepared in Maxpar Cell Staining Buffer (CSB; Fluidigm), for 30 minutes at room temperature.
902 Cells were washed with CSB, fixed and permeabilized with Maxpar Fix I buffer (Fluidigm) for 10
903 minutes at room temperature, washed with 2 volumes of Maxpar Perm-S buffer (Fluidigm), and
904 incubated with metal-labelled antibodies for intracellular markers, prepared in Maxpar Perm-S
905 buffer, for 30 minutes at room temperature. The list of antibodies used is shown in Table S1.
906 Finally, samples were washed with CSB, incubated 10 minutes at room temperature with a 2%

907 paraformaldehyde solution, washed once more with CSB, and left at 4 °C in Maxpar Fix and Perm
908 buffer (Fluidigm) with 125 nM Cell-ID™ Intercalator Ir (Fluidigm) until acquisition. Samples were
909 acquired between 12 and 48 hours after staining. Right before acquisition, cells were washed with
910 CSB, followed by Maxpar Cell Acquisition Solution (CAS; Fluidigm). Cells were resuspended in
911 CAS with 1 mM EDTA to a final concentration of 1×10^6 cells/mL, flushed through a 35 μ M
912 strainer, and supplemented with 1/10 v/v EQ Four Element Calibration Beads (Fluidigm). Mass
913 cytometry was performed using a Helios CyTOF instrument (Fluidigm) operated with software
914 v7.0.8493. The CyTOF instrument was started, tuned, and cleaned according to the manufacturer's
915 protocol, and samples acquired with an injection speed of 30 μ L/minute.

916 **(iii) Mass cytometry data analysis**

917 Data was exported as flow-cytometry FCS file format, and pre-processed with CyTOF software
918 (v6.7.1014; Fluidigm) for normalization. Processed files were uploaded to the Cytobank platform
919 (<https://www.cytobank.org/>) for initial gating (Gaussian parameters and cells/beads, live/dead and
920 singlets/doublets discriminations). CD45⁺ populations were gated and exported in FCS file format
921 and analysed with RStudio software (<https://www.rstudio.com/>) and cytofkit package
922 (<https://github.com/JinmiaoChenLab/cytofkit>) for Phenograph clustering using the following
923 parameters: 10.000 cells/sample, cytofAsinh as transformation Method, Phenograph as cluster
924 method, k equal to 30 as Rphenograph, tsne as visualization method, a seed of 42.

925 **Statistical analysis.**

926 Statistical analyses were performed using one-way analysis of variance (ANOVA) with Bonferroni
927 corrections, the one-tailed t test, or, when the requirements were not met, the Mann-Whitney U test.
928 P values of <0.05 were considered statistically significant. Normality and equal variance
929 assumptions were tested with the Kolmogorov-Smirnov test and the Brown-Forsythe test,
930 respectively. All analyses were performed using GraphPad Prism for Windows (version 9.1.0)
931 software.

932 **ACKNOWLEDGEMENTS**

933 We thank the members of the J.A.B. and A.G.B. laboratories for their thoughtful discussions and
934 support with this project. This work was supported by Biotechnology and Biological Sciences
935 Research Council (BBSRC, BB/T001976/1) funds to J.A.B., a joint BBSRC-Science Foundation
936 Ireland (SFI) grant to J.A.B. (BB/P020194/1) and A.G.B. (17/BBSRC/3414), and by SFI
937 (16/IA/4376) to A.G.B. The mass cytometry equipment at Queen's University Belfast was funded
938 by an institutional grant, and the technical support was provided by the Wellcome-Wolfson Institute
939 for Experimental Medicine.

940 **AUTHOR CONTRIBUTIONS**

941 Conceptualization, J.A.B. and A.G.B.; Investigation, C.F., J. sP., R. CG., L.G. B.G., J.L.I., M.C. and
942 A.D. Resources, R.S., R.J.I, A.K.; Funding acquisition, J.A.B. and A.G.B.; Writing original draft,
943 J.A.B. A.G.B. A.K. C.F.; Writing-Review and Editing M.C., R.J.I, A.K. J.A.B. and A.G.B.
944 Supervision, J.A.B., and A.G.B.

945 **DECLARATION OF INTERESTS**

946 The authors declare no competing interests

947 **REFERENCES**

948 Arnold, I.C., Mathisen, S., Schulthess, J., Danne, C., Hegazy, A.N., and Powrie, F. (2016). CD11c+
949 monocyte/macrophages promote chronic *Helicobacter hepaticus*-induced intestinal inflammation through
950 the production of IL-23. *Mucosal immunology* 9, 352-363.
951 Askarian, F., Van Sorge, N.M., Sangvik, M., Beasley, F.C., Henriksen, J.R., Sollid, J.U., Van Strijp, J.A., Nizet,
952 V., and Johannessen, M. (2014). A *Staphylococcus aureus* TIR domain protein virulence factor blocks TLR2-
953 mediated NF- κ B signaling. *Journal of innate immunity* 6, 485-498.
954 Bartholomew, T.L., Kidd, T.J., Sa Pessoa, J., Conde Alvarez, R., and Bengoechea, J.A. (2019). 2-Hydroxylation
955 of *Acinetobacter baumannii* Lipid A Contributes to Virulence. *Infect Immun* 87.
956 Belinda, L.W., Wei, W.X., Hanh, B.T., Lei, L.X., Bow, H., and Ling, D.J. (2008). SARM: a novel Toll-like receptor
957 adaptor, is functionally conserved from arthropod to human. *Mol Immunol* 45, 1732-1742.
958 Bengoechea, J.A., and Sa Pessoa, J. (2019). *Klebsiella pneumoniae* infection biology: living to counteract
959 host defences. *FEMS Microbiol Rev* 43, 123-144.
960 Bratkowski, M., Xie, T., Thayer, D.A., Lad, S., Mathur, P., Yang, Y.-S., Danko, G., Burdett, T.C., Danao, J., and
961 Cantor, A. (2020). Structural and mechanistic regulation of the pro-degenerative NAD hydrolase SARM1.
962 *Cell Reports* 32, 107999.

963 Broug-Holub, E., Toews, G.B., van Iwaarden, J.F., Strieter, R.M., Kunkel, S.L., Paine, R., 3rd, and Standiford,
964 T.J. (1997). Alveolar macrophages are required for protective pulmonary defenses in murine *Klebsiella*
965 pneumonia: elimination of alveolar macrophages increases neutrophil recruitment but decreases bacterial
966 clearance and survival. *Infect Immun* *65*, 1139-1146.

967 Cai, S., Batra, S., Shen, L., Wakamatsu, N., and Jeyaseelan, S. (2009). Both TRIF- and MyD88-dependent
968 signaling contribute to host defense against pulmonary *Klebsiella* infection. *J Immunol* *183*, 6629-6638.

969 Cai, S., Batra, S., Wakamatsu, N., Pacher, P., and Jeyaseelan, S. (2012). NLRC4 inflammasome-mediated
970 production of IL-1beta modulates mucosal immunity in the lung against gram-negative bacterial infection. *J*
971 *Immunol* *188*, 5623-5635.

972 Cai, X., Chen, J., Xu, H., Liu, S., Jiang, Q.X., Halfmann, R., and Chen, Z.J. (2014). Prion-like polymerization
973 underlies signal transduction in antiviral immune defense and inflammasome activation. *Cell* *156*, 1207-
974 1222.

975 Cano, V., March, C., Insua, J.L., Aguilo, N., Llobet, E., Moranta, D., Regueiro, V., Brennan, G.P., Millan-Lou,
976 M.I., Martin, C., *et al.* (2015). *Klebsiella pneumoniae* survives within macrophages by avoiding delivery to
977 lysosomes. *Cel Microbiol* *17*, 1537-1560.

978 Carlsson, E., Ding, J.L., and Byrne, B. (2016). SARM modulates MyD88-mediated TLR activation through BB-
979 loop dependent TIR-TIR interactions. *Biochimica et Biophysica Acta (BBA)-Molecular Cell Research* *1863*,
980 244-253.

981 Carty, M., Goodbody, R., Schroder, M., Stack, J., Moynagh, P.N., and Bowie, A.G. (2006). The human
982 adaptor SARM negatively regulates adaptor protein TRIF-dependent Toll-like receptor signaling. *Nat*
983 *Immunol* *7*, 1074-1081.

984 Carty, M., Kearney, J., Shanahan, K.A., Hams, E., Sugisawa, R., Connolly, D., Doran, C.G., Munoz-Wolf, N.,
985 Gurtler, C., Fitzgerald, K.A., *et al.* (2019). Cell Survival and Cytokine Release after Inflammasome Activation
986 Is Regulated by the Toll-IL-1R Protein SARM. *Immunity* *50*, 1412-1424 e1416.

987 Chang, E.Y., Guo, B., Doyle, S.E., and Cheng, G. (2007). Cutting edge: involvement of the type I IFN
988 production and signaling pathway in lipopolysaccharide-induced IL-10 production. *J Immunol* *178*, 6705-
989 6709.

990 Cirl, C., Wieser, A., Yadav, M., Duerr, S., Schubert, S., Fischer, H., Stappert, D., Wantia, N., Rodriguez, N.,
991 Wagner, H., *et al.* (2008). Subversion of Toll-like receptor signaling by a unique family of bacterial
992 Toll/interleukin-1 receptor domain-containing proteins. *Nat Med* *14*, 399-406.

993 Coll, R.C., Robertson, A.A., Chae, J.J., Higgins, S.C., Munoz-Planillo, R., Inserra, M.C., Vetter, I., Dungan, L.S.,
994 Monks, B.G., Stutz, A., *et al.* (2015). A small-molecule inhibitor of the NLRP3 inflammasome for the
995 treatment of inflammatory diseases. *Nat Med* *21*, 248-255.

996 Coronas-Serna, J.M., Louche, A., Rodríguez-Escudero, M., Roussin, M., Imbert, P.R., Rodríguez-Escudero, I.,
997 Terradot, L., Molina, M., Gorvel, J.-P., and Cid, V.J. (2020). The TIR-domain containing effectors BtpA and
998 BtpB from *Brucella abortus* impact NAD metabolism. *PLoS pathogens* *16*, e1007979.

999 Cortes, G., Borrell, N., de Astorza, B., Gomez, C., Sauleda, J., and Alberti, S. (2002). Molecular analysis of the
1000 contribution of the capsular polysaccharide and the lipopolysaccharide O side chain to the virulence of
1001 *Klebsiella pneumoniae* in a murine model of pneumonia. *Infect Immun* *70*, 2583-2590.

1002 DiAntonio, A. (2019). Axon degeneration: mechanistic insights lead to therapeutic opportunities for the
1003 prevention and treatment of peripheral neuropathy. *Pain* *160 Suppl 1*, S17-S22.

1004 Dong, C., Davis, R.J., and Flavell, R.A. (2002). MAP kinases in the immune response. *Ann Rev Immunol* *20*,
1005 55-72.

1006 Doran, C.G., Sugisawa, R., Carty, M., Roche, F., Fergus, C., Hokamp, K., Kelly, V.P., and Bowie, A.G. (2021).
1007 Next generation SARM1 knockout and epitope tagged CRISPR-Cas9-generated isogenic mice reveal that
1008 SARM1 does not participate in regulating nuclear transcription, despite confirmation of protein expression
1009 in macrophages. *bioRxiv*, 2021.2008.2025.457655.

1010 Fernandes-Alnemri, T., Yu, J.-W., Datta, P., Wu, J., and Alnemri, E.S. (2009). AIM2 activates the
1011 inflammasome and cell death in response to cytoplasmic DNA. *Nature* *458*, 509-513.

1012 Fernandes-Alnemri, T., Yu, J.-W., Juliana, C., Solorzano, L., Kang, S., Wu, J., Datta, P., McCormick, M., Huang,
1013 L., and McDermott, E. (2010). The AIM2 inflammasome is critical for innate immunity to *Francisella*
1014 *tularensis*. *Nat Immunol* *11*, 385-393.

- 1015 Fitzgerald, K.A., McWhirter, S.M., Faia, K.L., Rowe, D.C., Latz, E., Golenbock, D.T., Coyle, A.J., Liao, S.-M., and
1016 Maniatis, T. (2003). IKK ϵ and TBK1 are essential components of the IRF3 signaling pathway. *Nat Immunol* *4*,
1017 491-496.
- 1018 Fornarino, S., Laval, G., Barreiro, L.B., Manry, J., Vasseur, E., and Quintana-Murci, L. (2011). Evolution of the
1019 TIR domain-containing adaptors in humans: swinging between constraint and adaptation. *Mol Biol Evol* *28*,
1020 3087-3097.
- 1021 Frank, C.G., Reguerio, V., Rother, M., Moranta, D., Maeurer, A.P., Garmendia, J., Meyer, T.F., and
1022 Bengoechea, J.A. (2013). *Klebsiella pneumoniae* targets an EGF receptor-dependent pathway to subvert
1023 inflammation. *Cel Microbiol* *15*, 1212-1233.
- 1024 Ge, J., Gong, Y.N., Xu, Y., and Shao, F. (2012). Preventing bacterial DNA release and absent in melanoma 2
1025 inflammasome activation by a *Legionella* effector functioning in membrane trafficking. *Proc Natl Acad Sci U*
1026 *S A* *109*, 6193-6198.
- 1027 Giske, C.G., Monnet, D.L., Cars, O., Carmeli, Y., and ReAct-Action on Antibiotic, R. (2008). Clinical and
1028 economic impact of common multidrug-resistant gram-negative bacilli. *Antimicrob Agents Chemother* *52*,
1029 813-821.
- 1030 Greenberger, M.J., Strieter, R.M., Kunkel, S.L., Danforth, J.M., Goodman, R.E., and Standiford, T.J. (1995).
1031 Neutralization of IL-10 increases survival in a murine model of *Klebsiella pneumoniae*. *J Immunol* *155*, 722-
1032 729.
- 1033 Gu, D., Dong, N., Zheng, Z., Lin, D., Huang, M., Wang, L., Chan, E.W., Shu, L., Yu, J., Zhang, R., *et al.* (2018). A
1034 fatal outbreak of ST11 carbapenem-resistant hypervirulent *Klebsiella pneumoniae* in a Chinese hospital: a
1035 molecular epidemiological study. *Lancet Infectious diseases* *18*, 37-46.
- 1036 Hansen, K., Prabakaran, T., Laustsen, A., Jorgensen, S.E., Rahbaek, S.H., Jensen, S.B., Nielsen, R., Leber, J.H.,
1037 Decker, T., Horan, K.A., *et al.* (2014). *Listeria monocytogenes* induces IFN β expression through an IFI16-,
1038 cGAS- and STING-dependent pathway. *EMBO J* *33*, 1654-1666.
- 1039 Henry, T., Brotcke, A., Weiss, D.S., Thompson, L.J., and Monack, D.M. (2007). Type I interferon signaling is
1040 required for activation of the inflammasome during *Francisella* infection. *J Exp Med* *204*, 987-994.
- 1041 Holt, K.E., Wertheim, H., Zadoks, R.N., Baker, S., Whitehouse, C.A., Dance, D., Jenney, A., Connor, T.R., Hsu,
1042 L.Y., Severin, J., *et al.* (2015). Genomic analysis of diversity, population structure, virulence, and
1043 antimicrobial resistance in *Klebsiella pneumoniae*, an urgent threat to public health. *Proc Natl Acad Sci U S*
1044 *A* *112*, E3574-3581.
- 1045 Horsefield, S., Burdett, H., Zhang, X., Manik, M.K., Shi, Y., Chen, J., Qi, T., Gilley, J., Lai, J.S., Rank, M.X., *et al.*
1046 (2019). NAD(+) cleavage activity by animal and plant TIR domains in cell death pathways. *Science* *365*, 793-
1047 799.
- 1048 Hua, K.-F., Yang, F.-L., Chiu, H.-W., Chou, J.-C., Dong, W.-C., Lin, C.-N., Lin, C.-Y., Wang, J.-T., Li, L.-H., and
1049 Chiu, H.-W. (2015). Capsular polysaccharide is involved in NLRP3 inflammasome activation by *Klebsiella*
1050 *pneumoniae* serotype K1. *Infect Immun* *83*, 3396-3409.
- 1051 Hughes, R.O., Bosanac, T., Mao, X., Engber, T.M., DiAntonio, A., Milbrandt, J., Devraj, R., and Krauss, R.
1052 (2021). Small Molecule SARM1 Inhibitors Recapitulate the SARM1(-/-) Phenotype and Allow Recovery of a
1053 Metastable Pool of Axons Fated to Degenerate. *Cell Rep* *34*, 108588.
- 1054 Imbert, P.R., Louche, A., Luizet, J.B., Grandjean, T., Bigot, S., Wood, T.E., Gagné, S., Blanco, A., Wunderley,
1055 L., and Terradot, L. (2017). A *Pseudomonas aeruginosa* TIR effector mediates immune evasion by targeting
1056 UBAP 1 and TLR adaptors. *EMBO J* *36*, 1869-1887.
- 1057 Ivashkiv, L.B., and Donlin, L.T. (2014). Regulation of type I interferon responses. *Nat Rev Immunol* *14*, 36-49.
- 1058 Ivin, M., Dumigan, A., de Vasconcelos, F.N., Ebner, F., Borroni, M., Kavirayani, A., Przybyszewska, K.N.,
1059 Ingram, R.J., Lienenklaus, S., Kalinke, U., *et al.* (2017). Natural killer cell-intrinsic type I IFN signaling controls
1060 *Klebsiella pneumoniae* growth during lung infection. *PLoS pathogens* *13*, e1006696.
- 1061 Jenner, R.G., and Young, R.A. (2005). Insights into host responses against pathogens from transcriptional
1062 profiling. *Nat Rev Microbiol* *3*, 281-294.
- 1063 Jones, J.W., Kayagaki, N., Broz, P., Henry, T., Newton, K., O'Rourke, K., Chan, S., Dong, J., Qu, Y., and Roose-
1064 Girma, M. (2010). Absent in melanoma 2 is required for innate immune recognition of *Francisella*
1065 *tuhalensis*. *Proc Natl Acad Sci U S A* *107*, 9771-9776.

1066 Kidd, T.J., Mills, G., Sa-Pessoa, J., Dumigan, A., Frank, C.G., Insua, J.L., Ingram, R., Hobley, L., and
1067 Bengoechea, J.A. (2017). A *Klebsiella pneumoniae* antibiotic resistance mechanism that subdues host
1068 defences and promotes virulence. *EMBO Mol Med* **9**, 430-447.

1069 Kuijl, C., Savage, N.D., Marsman, M., Tuin, A.W., Janssen, L., Egan, D.A., Ketema, M., van den Nieuwendijk,
1070 R., van den Eeden, S.J., Geluk, A., *et al.* (2007). Intracellular bacterial growth is controlled by a kinase
1071 network around PKB/AKT1. *Nature* **450**, 725-730.

1072 Kyei, G.B., Vergne, I., Chua, J., Roberts, E., Harris, J., Junutula, J.R., and Deretic, V. (2006). Rab14 is critical
1073 for maintenance of *Mycobacterium tuberculosis* phagosome maturation arrest. *EMBO J* **25**, 5250-5259.

1074 Lam, M.M.C., Wick, R.R., Wyres, K.L., Gorrie, C.L., Judd, L.M., Jenney, A.W.J., Brisse, S., and Holt, K.E. (2018).
1075 Genetic diversity, mobilisation and spread of the yersiniabactin-encoding mobile element ICEKp in
1076 *Klebsiella pneumoniae* populations. *Microbial genomics*.

1077 Lawlor, M.S., Hsu, J., Rick, P.D., and Miller, V.L. (2005). Identification of *Klebsiella pneumoniae* virulence
1078 determinants using an intranasal infection model. *Mol Microbiol* **58**, 1054-1073.

1079 Lery, L.M., Frangeul, L., Tomas, A., Passet, V., Almeida, A.S., Bialek-Davenet, S., Barbe, V., Bengoechea, J.A.,
1080 Sansonetti, P., Brisse, S., *et al.* (2014). Comparative analysis of *Klebsiella pneumoniae* genomes identifies a
1081 phospholipase D family protein as a novel virulence factor. *BMC biology* **12**, 41-7007-7012-7041.

1082 Levine, J.H., Simonds, E.F., Bendall, S.C., Davis, K.L., Amir el, A.D., Tadmor, M.D., Litvin, O., Fienberg, H.G.,
1083 Jager, A., Zunder, E.R., *et al.* (2015). Data-Driven Phenotypic Dissection of AML Reveals Progenitor-like Cells
1084 that Correlate with Prognosis. *Cell* **162**, 184-197.

1085 Lewis, S.M., Treacher, D.F., Edgeworth, J., Mahalingam, G., Brown, C.S., Mare, T.A., Stacey, M., Beale, R.,
1086 and Brown, K.A. (2015). Expression of CD11c and EMR2 on neutrophils: potential diagnostic biomarkers for
1087 sepsis and systemic inflammation. *Clin Exp Immunol* **182**, 184-194.

1088 Lipworth, S., Vihta, K.-D., Chau, K., Barker, L., George, S., Kavanagh, J., Davies, T., Vaughan, A., Andersson,
1089 M., Jeffery, K., *et al.* (2021). Ten-year longitudinal molecular epidemiology study of *Escherichia coli* and
1090 *Klebsiella* species bloodstream infections in Oxfordshire, UK. *Genome Medicine* **13**, 144.

1091 Lu, A., Magupalli, V.G., Ruan, J., Yin, Q., Atianand, M.K., Vos, M.R., Schroder, G.F., Fitzgerald, K.A., Wu, H.,
1092 and Egelman, E.H. (2014). Unified polymerization mechanism for the assembly of ASC-dependent
1093 inflammasomes. *Cell* **156**, 1193-1206.

1094 Magiorakos, A.-P., Suetens, C., Monnet, D.L., Gagliotti, C., and Heuer, O.E. (2013). The rise of carbapenem
1095 resistance in Europe: just the tip of the iceberg? *Antimicrobial resistance and infection control* **2**, 1-3.

1096 Man, S.M., Karki, R., Malireddi, R.S., Neale, G., Vogel, P., Yamamoto, M., Lamkanfi, M., and Kanneganti, T.-
1097 D. (2015). The transcription factor IRF1 and guanylate-binding proteins target activation of the AIM2
1098 inflammasome by Francisella infection. *Nat Immunol* **16**, 467-475.

1099 March, C., Cano, V., Moranta, D., Llobet, E., Perez-Gutierrez, C., Tomas, J.M., Suarez, T., Garmendia, J., and
1100 Bengoechea, J.A. (2013). Role of bacterial surface structures on the interaction of *Klebsiella pneumoniae*
1101 with phagocytes. *PLoS one* **8**, e56847.

1102 McNab, F.W., Ewbank, J., Howes, A., Moreira-Teixeira, L., Martirosyan, A., Ghilardi, N., Saraiva, M., and
1103 O'Garra, A. (2014). Type I IFN induces IL-10 production in an IL-27-independent manner and blocks
1104 responsiveness to IFN-gamma for production of IL-12 and bacterial killing in *Mycobacterium tuberculosis*-
1105 infected macrophages. *J Immunol* **193**, 3600-3612.

1106 Motani, K., Kushiya, H., Imamura, R., Kinoshita, T., Nishiuchi, T., and Suda, T. (2011). Caspase-1 protein
1107 induces apoptosis-associated speck-like protein containing a caspase recruitment domain (ASC)-mediated
1108 necrosis independently of its catalytic activity. *J Biol Chem* **286**, 33963-33972.

1109 Nassif, X., Fournier, J.M., Arondel, J., and Sansonetti, P.J. (1989). Mucoid phenotype of *Klebsiella*
1110 *pneumoniae* is a plasmid-encoded virulence factor. *Infect Immun* **57**, 546-552.

1111 O'Neill, L.A., and Bowie, A.G. (2007). The family of five: TIR-domain-containing adaptors in Toll-like receptor
1112 signalling. *Nat Rev Immunol* **7**, 353-364.

1113 Ostrowski, P.P., Fairn, G.D., Grinstein, S., and Johnson, D.E. (2016). Cresyl violet: a superior fluorescent
1114 lysosomal marker. *Traffic* **17**, 1313-1321.

1115 Pattison, M.J., MacKenzie, K.F., and Arthur, J.S.C. (2012). Inhibition of JAKs in macrophages increases
1116 lipopolysaccharide-induced cytokine production by blocking IL-10-mediated feedback. *J Immunol* **189**,
1117 2784-2792.

- 1118 Penalva, G., Hogberg, L.D., Weist, K., Vlahovic-Palcevski, V., Heuer, O., Monnet, D.L., Group, E.S.-N.S., and
1119 Group, E.A.-N.S. (2019). Decreasing and stabilising trends of antimicrobial consumption and resistance in
1120 *Escherichia coli* and *Klebsiella pneumoniae* in segmented regression analysis, European Union/European
1121 Economic Area, 2001 to 2018. *Euro Surveill* **24**.
- 1122 Peng, J., Yuan, Q., Lin, B., Panneerselvam, P., Wang, X., Luan, X.L., Lim, S.K., Leung, B.P., Ho, B., and Ding, J.L.
1123 (2010). SARM inhibits both TRIF-and MyD88-mediated AP-1 activation. *Eur J Immunol* **40**, 1738-1747.
- 1124 Rathinam, V.A., Jiang, Z., Waggoner, S.N., Sharma, S., Cole, L.E., Waggoner, L., Vanaja, S.K., Monks, B.G.,
1125 Ganesan, S., Latz, E., *et al.* (2010). The AIM2 inflammasome is essential for host defense against cytosolic
1126 bacteria and DNA viruses. *Nat Immunol* **11**, 395-402.
- 1127 Regueiro, V., Moranta, D., Frank, C.G., Larrarte, E., Margareto, J., March, C., Garmendia, J., and
1128 Bengoechea, J.A. (2011). *Klebsiella pneumoniae* subverts the activation of inflammatory responses in a
1129 NOD1-dependent manner. *Cel Microbiol* **13**, 135-153.
- 1130 Rusinova, I., Forster, S., Yu, S., Kannan, A., Mase, M., Cumming, H., Chapman, R., and Hertzog, P.J. (2013).
1131 Interferome v2.0: an updated database of annotated interferon-regulated genes. *Nucleic Acids Res* **41**,
1132 D1040-1046.
- 1133 Sa-Pessoa, J., Przybyszewska, K., Vasconcelos, F.N., Dumigan, A., Frank, C.G., Hobley, L., and Bengoechea,
1134 J.A. (2020). *Klebsiella pneumoniae* Reduces SUMOylation To Limit Host Defense Responses. *mBio* **11**.
- 1135 Saraiva, M., and O'Garra, A. (2010). The regulation of IL-10 production by immune cells. *Nat Rev Immunol*
1136 **10**, 170-181.
- 1137 Schlam, D., Bagshaw, R.D., Freeman, S.A., Collins, R.F., Pawson, T., Fairn, G.D., and Grinstein, S. (2015).
1138 Phosphoinositide 3-kinase enables phagocytosis of large particles by terminating actin assembly through
1139 Rac/Cdc42 GTPase-activating proteins. *Nat Comms* **6**, 8623.
- 1140 Secombes, C.J., and Zou, J. (2017). Evolution of Interferons and Interferon Receptors. *Front Immunol* **8**, 209.
- 1141 Sester, D.P., Thygesen, S.J., Sagulenko, V., Vajjhala, P.R., Cridland, J.A., Vitak, N., Chen, K.W., Osborne, G.W.,
1142 Schroder, K., and Stacey, K.J. (2015). A novel flow cytometric method to assess inflammasome formation. *J*
1143 *Immunol* **194**, 455-462.
- 1144 Shi, H., Murray, A., and Beutler, B. (2016). Reconstruction of the Mouse Inflammasome System in HEK293T
1145 Cells. *Bio Protoc* **6**.
- 1146 Szretter, K.J., Samuel, M.A., Gilfillan, S., Fuchs, A., Colonna, M., and Diamond, M.S. (2009). The immune
1147 adaptor molecule SARM modulates tumor necrosis factor alpha production and microglia activation in the
1148 brainstem and restricts West Nile Virus pathogenesis. *J Virol* **83**, 9329-9338.
- 1149 Taniguchi, K., and Karin, M. (2018). NF-kappaB, inflammation, immunity and cancer: coming of age. *Nat Rev*
1150 *Immunol* **18**, 309-324.
- 1151 Tomas, A., Lery, L., Regueiro, V., Perez-Gutierrez, C., Martinez, V., Moranta, D., Llobet, E., Gonzalez-Nicolau,
1152 M., Insua, J.L., Tomas, J.M., *et al.* (2015). Functional Genomic Screen Identifies *Klebsiella pneumoniae*
1153 Factors Implicated in Blocking Nuclear Factor kappaB (NF-kappaB) Signaling. *J Biol Chem* **290**, 16678-16697.
- 1154 Tsuchiya, K., Hara, H., Kawamura, I., Nomura, T., Yamamoto, T., Daim, S., Dewamitta, S.R., Shen, Y., Fang,
1155 R., and Mitsuyama, M. (2010). Involvement of absent in melanoma 2 in inflammasome activation in
1156 macrophages infected with *Listeria monocytogenes*. *J Immunol* **185**, 1186-1195.
- 1157 Uccellini, M.B., Bardina, S.V., Sánchez-Aparicio, M.T., White, K.M., Hou, Y.-J., Lim, J.K., and García-Sastre, A.
1158 (2020). Passenger mutations confound phenotypes of SARM1-deficient mice. *Cell reports* **31**, 107498.
- 1159 Uhlen, M., Oksvold, P., Fagerberg, L., Lundberg, E., Jonasson, K., Forsberg, M., Zwahlen, M., Kampf, C.,
1160 Wester, K., and Hober, S. (2010). Towards a knowledge-based human protein atlas. *Nat Biotech* **28**, 1248-
1161 1250.
- 1162 Ulland, T.K., Buchan, B.W., Ketterer, M.R., Fernandes-Alnemri, T., Meyerholz, D.K., Apicella, M.A., Alnemri,
1163 E.S., Jones, B.D., Nauseef, W.M., and Sutterwala, F.S. (2010). Cutting edge: mutation of *Francisella*
1164 *tularensis* *mvnN* leads to increased macrophage absent in melanoma 2 inflammasome activation and a loss
1165 of virulence. *J Immunol* **185**, 2670-2674.
- 1166 Wang, P.-H., Ye, Z.-W., Deng, J.-J., Siu, K.-L., Gao, W.-W., Chaudhary, V., Cheng, Y., Fung, S.-Y., Yuen, K.-S.,
1167 Ho, T.-H., *et al.* (2018). Inhibition of AIM2 inflammasome activation by a novel transcript isoform of IFI16.
1168 *EMBO Rep* **19**, e45737.

- 1169 Wieland, C.W., van Lieshout, M.H., Hoogendijk, A.J., and van der Poll, T. (2011). Host defence during
1170 *Klebsiella pneumoniae* relies on haematopoietic-expressed Toll-like receptors 4 and 2. *Eur Respir J* 37, 848-
1171 857.
- 1172 Willingham, S.B., Allen, I.C., Bergstralh, D.T., Brickey, W.J., Huang, M.T.-H., Taxman, D.J., Duncan, J.A., and
1173 Ting, J.P.-Y. (2009a). NLRP3 (NALP3, Cryopyrin) facilitates in vivo caspase-1 activation, necrosis, and HMGB1
1174 release via inflammasome-dependent and-independent pathways. *J Immunol* 183, 2008-2015.
- 1175 Willingham, S.B., Allen, I.C., Bergstralh, D.T., Brickey, W.J., Huang, M.T., Taxman, D.J., Duncan, J.A., and
1176 Ting, J.P. (2009b). NLRP3 (NALP3, Cryopyrin) facilitates in vivo caspase-1 activation, necrosis, and HMGB1
1177 release via inflammasome-dependent and -independent pathways. *J Immunol* 183, 2008-2015.
- 1178 Xiong, D., Song, L., Geng, S., Jiao, Y., Zhou, X., Song, H., Kang, X., Zhou, Y., Xu, X., and Sun, J. (2019).
1179 *Salmonella* coiled-coil-and TIR-containing Tcps evades the innate immune system and subdues
1180 inflammation. *Cell reports* 28, 804-818. e807.
- 1181 Xiong, H., Carter, R.A., Leiner, I.M., Tang, Y.W., Chen, L., Kreiswirth, B.N., and Pamer, E.G. (2015). Distinct
1182 Contributions of Neutrophils and CCR2+ Monocytes to Pulmonary Clearance of Different *Klebsiella*
1183 *pneumoniae* Strains. *Infect Immun* 83, 3418-3427.
- 1184 Xiong, H., Keith, J.W., Samilo, D.W., Carter, R.A., Leiner, I.M., and Pamer, E.G. (2016). Innate
1185 Lymphocyte/Ly6C(hi) Monocyte Crosstalk Promotes *Klebsiella Pneumoniae* Clearance. *Cell* 165, 679-689.
- 1186 Yao, H., Qin, S., Chen, S., Shen, J., and Du, X.D. (2018). Emergence of carbapenem-resistant hypervirulent
1187 *Klebsiella pneumoniae*. *Lancet Infectious diseases* 18, 25-3099(3017)30628-X.
- 1188 Ye, P., Rodriguez, F.H., Kanaly, S., Stocking, K.L., Schurr, J., Schwarzenberger, P., Oliver, P., Huang, W.,
1189 Zhang, P., Zhang, J., *et al.* (2001). Requirement of interleukin 17 receptor signaling for lung CXC chemokine
1190 and granulocyte colony-stimulating factor expression, neutrophil recruitment, and host defense. *J Exp Med*
1191 194, 519-527.
- 1192 Yin, Q., Sester, D.P., Tian, Y., Hsiao, Y.S., Lu, A., Cridland, J.A., Sagulenko, V., Thygesen, S.J., Choubey, D.,
1193 Hornung, V., *et al.* (2013). Molecular mechanism for p202-mediated specific inhibition of AIM2
1194 inflammasome activation. *Cell Rep* 4, 327-339.
- 1195 Zhang, Q., Zmasek, C.M., Cai, X., and Godzik, A. (2011). TIR domain-containing adaptor SARM is a late
1196 addition to the ongoing microbe-host dialog. *Dev Comp Immunol* 35, 461-468.
- 1197 Zhang, Y., Zeng, J., Liu, W., Zhao, F., Hu, Z., Zhao, C., Wang, Q., Wang, X., Chen, H., Li, H., *et al.* (2015).
1198 Emergence of a hypervirulent carbapenem-resistant *Klebsiella pneumoniae* isolate from clinical infections
1199 in China. *J Infect* 71, 553-560.
- 1200 Zhang, Y., Zhao, C., Wang, Q., Wang, X., Chen, H., Li, H., Zhang, F., Li, S., Wang, R., and Wang, H. (2016).
1201 High Prevalence of Hypervirulent *Klebsiella pneumoniae* Infection in China: Geographic Distribution, Clinical
1202 Characteristics, and Antimicrobial Resistance. *Antimicrob Agents Chemother* 60, 6115-6120.

1203

1204

1205

1206 **FIGURE LEGENDS**

1207 **Figure 1. SARM1 negatively regulates *K. pneumoniae*-induced inflammation.**

1208 A. ELISA of TNF α , IL1 β , CXCL10 secreted by wild-type (WT) and *sarm1*^{-/-} macrophages non-
1209 infected (ni) or infected with Kp52145 for 6 and 16 h. Type I IFN levels determined in the
1210 supernatants of macrophages 16 h post infection. The reporter cell line B16-Blue IFN- α/β was used

1211 for the quantification of levels of SEAP produced upon stimulation of the supernatants with the
1212 detection medium QUANTI-Blue and presented as OD₆₅₅. After 1 h contact, the medium was
1213 replaced with medium containing gentamicin (100 µg/ml) to kill extracellular bacteria.

1214 B. Immunoblot analysis of ISG15, Viperin and tubulin levels in lysates of wild-type (WT) and
1215 *sarm1*^{-/-} macrophages non-infected (NI) or infected with Kp52145 for the indicated time points.
1216 After 1 h contact, the medium was replaced with medium containing gentamicin (100 µg/ml) to kill
1217 extracellular bacteria.

1218 C. ELISA of TNFα, IL1β, CXCL10 secreted by wild-type (WT) macrophages, and retrovirally
1219 transfected *sarm1*^{-/-} cells with FLAG-SARM1 or control vector (EV) non-infected (ni) or infected
1220 with Kp52145 (Kp) for 16 h. After 1 h contact, the medium was replaced with medium containing
1221 gentamicin (100 µg/ml) to kill extracellular bacteria.

1222 D. *il1b*, *tnfa*, *cxcl10*, *isg15*, *ifit1*, and *mx1* mRNA levels were assessed by qPCR, in wild-type (WT)
1223 and *sarm1*^{-/-} macrophages non-infected (ni) or infected with Kp52145 for 6 and 16 h. After 1 h
1224 contact, the medium was replaced with medium containing gentamicin (100 µg/ml) to kill
1225 extracellular bacteria.

1226 E. Immunoblot analysis of phosphorylated Iκκ α /β (P-Iκκ), phosphorylated IκB α (P-IκB α), total
1227 IκB α (IκB α) and tubulin levels in lysates of wild-type (WT) and *sarm1*^{-/-} macrophages non-infected
1228 (NI) or infected with Kp52145 for the indicated time points. After 1 h contact, the medium was
1229 replaced with medium containing gentamicin (100 µg/ml) to kill extracellular bacteria.

1230 F. Immunoblot analysis of phosphorylated TBK1 (P-TBK1), phosphorylated Irf3 (P-IRF3) and
1231 tubulin levels in lysates of wild-type (WT) and *sarm1*^{-/-} macrophages non-infected (NI) or infected
1232 with Kp52145 for the indicated time points. After 1 h contact, the medium was replaced with
1233 medium containing gentamicin (100 µg/ml) to kill extracellular bacteria.

1234 G. *Sarm1*^{FLAG} macrophages were transfected with a MyD88-HA or TRIF-HA plasmids, and the
1235 following day infected with Kp52145. Cells were lysed in RIPA buffer, and lysates
1236 immunoprecipitated using anti-FLAG antibody. Preimmune mouse IgG served as negative control.

1237 H. Immunoblot analysis of phosphorylated ERK (P-ERK), phosphorylated JNK (P-JNK
1238 phosphorylated p38 (P-p38) and tubulin levels in lysates of wild-type (WT) and *sarm1*^{-/-}
1239 macrophages non-infected (NI) or infected with Kp52145 for the indicated time points.

1240 In panels B, E, F, G, and H images are representative of three independent experiments. In panels
1241 A, C and D values are presented as the mean \pm SD of three independent experiments measured in
1242 duplicate. ****P \leq 0.0001; ***P \leq 0.001; ** P \leq 0.01; *P \leq 0.05 for the indicated comparisons
1243 determined using one way-ANOVA with Bonferroni contrast for multiple comparisons test.

1244 **Figure 2. SARM1 is required for *K. pneumoniae* induction of IL10 via p38.**

1245 A. *il10* mRNA levels were assessed by qPCR, in wild-type (WT) and *sarm1*^{-/-} macrophages non-
1246 infected (ni) or infected with Kp52145 for 6 and 16 h. After 1 h contact, the medium was replaced
1247 with medium containing gentamicin (100 μ g/ml) to kill extracellular bacteria.

1248 B. ELISA of IL10 secreted by wild-type (WT) and *sarm1*^{-/-} macrophages non-infected (ni) or
1249 infected with Kp52145 for 16 h. After 1 h contact, the medium was replaced with medium
1250 containing gentamicin (100 μ g/ml) to kill extracellular bacteria.

1251 C. Immunoblot analysis of phosphorylated STAT3 (P-STAT3), total STAT3 (STAT3) and tubulin
1252 levels in lysates of wild-type (WT) and *sarm1*^{-/-} macrophages non-infected (NI) or infected with
1253 Kp52145 for the indicated time points. After 1 h contact, the medium was replaced with medium
1254 containing gentamicin (100 μ g/ml) to kill extracellular bacteria.

1255 D. ELISA of TNF α , IL1 β , CXCL10 secreted by wild-type (WT) and *sarm1*^{-/-} macrophages non-
1256 infected or infected with Kp52145 for 16 h. Where indicated, cells were treated with recombinant
1257 IL10 (1 ng/ml) overnight before infection. After 1 h contact, the medium was replaced with medium
1258 containing gentamicin (100 μ g/ml) to kill extracellular bacteria.

1259 E. *il1b*, *tnfa*, and *cxcl10* mRNA levels were assessed by qPCR in *il10*^{-/-} macrophages, and *il10*^{-/-}
1260 cells transfected with All Stars siRNA control (AS), or SARM1 siRNA (siSARM) non-infected
1261 (ni) or infected with Kp52145 (Kp) for 16 h.

1262 F. Immunoblot analysis of phosphorylated p38 (P-p38), and tubulin levels in lysates of *sarm1*^{-/-}
1263 macrophages treated with isotype control antibody, or IFNAR1 blocking non-infected (NI) or
1264 infected with Kp52145 for the indicated time points. After 1 h contact, the medium was replaced
1265 with medium containing gentamicin (100 µg/ml) to kill extracellular bacteria.

1266 G. Immunoblot analysis of phosphorylated p38 (P-p38), and tubulin levels in lysates of wild-type
1267 macrophages (WT) treated with isotype control antibody, or IFNAR1 blocking non-infected (NI) or
1268 infected with Kp52145 for the indicated time points. After 1 h contact, the medium was replaced
1269 with medium containing gentamicin (100 µg/ml) to kill extracellular bacteria.

1270 H. ELISA of IL10, secreted by wild-type (WT) and *sarm1*^{-/-} macrophages non-infected or infected
1271 with Kp52145 for 16 h. Where indicated, cells were treated with isotype control antibody, or
1272 IFNAR1 blocking overnight before infection. After 1 h contact, the medium was replaced with
1273 medium containing gentamicin (100 µg/ml) to kill extracellular bacteria.

1274 I. ELISA of IL1β, and TNFα secreted by wild-type (WT) and *sarm1*^{-/-} macrophages non-infected or
1275 infected with Kp52145 for 16 h. Where indicated, cells were treated with isotype control antibody,
1276 or IFNAR1 blocking overnight before infection. After 1 h contact, the medium was replaced with
1277 medium containing gentamicin (100 µg/ml) to kill extracellular bacteria.

1278 In panels C, F, and G images are representative of three independent experiments. In panels A, B,
1279 D, E, H and I values are presented as the mean ± SD of three independent experiments measured in
1280 duplicate. ****P ≤ 0.0001; ***P ≤ 0.001; ** P ≤ 0.01; ns, P > 0.05 for the indicated comparisons
1281 determined using one way-ANOVA with Bonferroni contrast for multiple comparisons test.

1282 **Figure 3. SARM1 negatively regulates *K. pneumoniae*-induced AIM2 inflammasome**
1283 **activation.**

1284 A. Immunoblot analysis of processed pro-IL1β, and β-actin levels in lysates of wild-type
1285 macrophages (WT) and *sarm1*^{-/-} macrophages non-infected (NI) or infected with Kp52145 for the
1286 indicated time points. After 1 h contact, the medium was replaced with medium containing
1287 gentamicin (100 µg/ml) to kill extracellular bacteria.

1288 B. Immunoblot analysis of processed caspase 1, and β -actin levels in lysates of wild-type
1289 macrophages (WT) and *sarm1*^{-/-} macrophages non-infected (NI) or infected with Kp52145 for the
1290 indicated time points. After 1 h contact, the medium was replaced with medium containing
1291 gentamicin (100 μ g/ml) to kill extracellular bacteria.

1292 C. Immunoblot analysis of cleaved gasdermin D (GSDMD), and β -actin levels in lysates of wild-
1293 type macrophages (WT) and *sarm1*^{-/-} macrophages non-infected (NI) or infected with Kp52145 for
1294 the indicated time points. After 1 h contact, the medium was replaced with medium containing
1295 gentamicin (100 μ g/ml) to kill extracellular bacteria.

1296 D. ELISA of IL1 β secreted by wild-type (WT) and *sarm1*^{-/-} macrophages non-infected (ni) or
1297 infected with Kp52145 for 6 and 16h. Cells were treated with the caspase-1 inhibitor YVAD or the
1298 DMSO vehicle solution. After 1 h contact, the medium was replaced with medium containing
1299 gentamicin (100 μ g/ml) to kill extracellular bacteria.

1300 E. Wild-type (WT), *sarm1*^{-/-}, *nlrp3*^{-/-}, and *aim2*^{-/-} macrophages were non-infected (ni) or infected
1301 with Kp52145 (Kp) for 16 h, and ASC specks were detected by flow cytometry. After 1 h contact,
1302 the medium was replaced with medium containing gentamicin (100 μ g/ml) to kill extracellular
1303 bacteria.

1304 F. ELISA of IL1 β secreted by wild-type (WT) and *aim2*^{-/-} macrophages non-infected (ni) or infected
1305 with Kp52145 for 6 and 16 h. After 1 h contact, the medium was replaced with medium containing
1306 gentamicin (100 μ g/ml) to kill extracellular bacteria.

1307 G. Immunoblot analysis of processed caspase 1, cleaved gasdermin D (GSDMD) and β -actin levels
1308 in lysates of wild-type macrophages (WT) and *aim2*^{-/-} macrophages non-infected (NI) or infected
1309 with Kp52145 for 16h. After 1 h contact, the medium was replaced with medium containing
1310 gentamicin (100 μ g/ml) to kill extracellular bacteria.

1311 H. ELISA of IL1 β secreted by *sarm1*^{-/-} macrophages treated with the NLRP3 inhibitor MCC950 or
1312 DMSO vehicle control, and *sarm1*^{-/-} cells transfected with All Stars siRNA control (AS), or Aim2
1313 siRNA (siAim2). Cells were non-infected (ni) or infected with Kp52145 (Kp) for 16 h. After 1 h

1314 contact, the medium was replaced with medium containing gentamicin (100 µg/ml) to kill
1315 extracellular bacteria.

1316 I. Reconstitution of AIM2 inflammasome activation in HEK293T cells by co-transfection of
1317 plasmids expressing HA-AIM2, ASC, procaspase-1, and pro-IL-1β. Plasmids expressing FLAG
1318 SARM1, FLAG SARM1 TIR, FLAG SARM1 ΔTIR (10, 50, 100ng), or empty vector (EV) were
1319 co-transfected. Secreted IL-1β in the culture supernatants was detected by ELISA. HA-AIM2 and
1320 FLAG SARM1 (or truncations) were detected by immunoblotting with anti-HA and anti-FLAG
1321 antibodies respectively.

1322 J. *Sarm1*^{-/-} iBMDMs expressing empty vector (EV) or FLAG-SARM1 were non-infected (NI) or
1323 infected with Kp52145 for 24 h. Cells were lysed by RIPA buffer and immunoprecipitation was
1324 performed using anti-FLAG (M2) beads. The immune complexes were detected by immunoblotting
1325 with anti-SARM1, anti-AIM2 antibodies.

1326 In panels A, B, C, G, and J images are representative of three independent experiments. In panels D,
1327 E, F, H, and I values are presented as the mean ± SD of three independent experiments measured in
1328 duplicate. ****P ≤ 0.0001; ***P ≤ 0.001; **P ≤ 0.01; *P ≤ 0.05; ns, P > 0.05 for the indicated
1329 comparisons determined using one way-ANOVA with Bonferroni contrast for multiple comparisons
1330 test.

1331 **Figure 4. *K. pneumoniae* induces AIM2 in a type I IFN-dependent manner.**

1332 A. *aim2* mRNA levels were assessed by qPCR in wild-type macrophages (WT) non-infected (ni) or
1333 infected with Kp52145 for 16 h. After 1 h contact, the medium was replaced with medium
1334 containing gentamicin (100 µg/ml) to kill extracellular bacteria.

1335 B. *aim2* mRNA levels were assessed by qPCR in the lungs of infected wild-type mice (WT) for 24
1336 h.

1337 C. Immunoblot analysis of AIM2 and β-actin levels in lysates of wild-type macrophages (WT)
1338 macrophages non-infected (NI) or infected with Kp52145 for the indicated time points. After 1 h

1339 contact, the medium was replaced with medium containing gentamicin (100 µg/ml) to kill
1340 extracellular bacteria.

1341 *D. aim2* mRNA levels were assessed by qPCR in wild-type (WT), and *ifnar1*^{-/-} macrophages non-
1342 infected (ni) or infected with Kp52145 for 16 h. Immunoblot analysis of Aim2 and β-actin levels in
1343 lysates of wild-type macrophages (WT) and *ifnar1*^{-/-} macrophages non-infected (NI) or infected
1344 with Kp52145 for the indicated time points. After 1 h contact, the medium was replaced with
1345 medium containing gentamicin (100 µg/ml) to kill extracellular bacteria.

1346 *E. aim2* mRNA levels were assessed by qPCR in wild-type macrophages (WT) non-infected (ni) or
1347 infected with Kp52145, the capsule mutant 52145- $\Delta manC$ (Δcps), the mutant lacking the LPS O-
1348 polysaccharide, 52145- Δglf (Δglf), and the double mutant lacking the CPS and the LPS O-
1349 polysaccharide, 52145- Δwca_{k2} - Δglf ($\Delta cps \Delta glf$) for 16 h. After 1 h contact, the medium was
1350 replaced with medium containing gentamicin (100 µg/ml) to kill extracellular bacteria.

1351 *F.* Immunoblot analysis of Aim2 and β-actin levels in lysates of wild-type macrophages (WT)
1352 macrophages non-infected (NI) or infected with Kp52145, the capsule mutant 52145- $\Delta manC$
1353 (Δcps), the mutant lacking the LPS O-polysaccharide, 52145- Δglf (Δglf), and the double mutant
1354 lacking the CPS and the LPS O-polysaccharide, 52145- Δwca_{k2} - Δglf ($\Delta cps \Delta glf$) for the indicated
1355 time points. After 1 h contact, the medium was replaced with medium containing gentamicin (100
1356 µg/ml) to kill extracellular bacteria.

1357 *G.* ELISA of IL1β secreted by wild-type macrophages non-infected (ni) or infected with Kp52145,
1358 the capsule mutant 52145- $\Delta manC$ (Δcps), the mutant lacking the LPS O-polysaccharide, 52145-
1359 Δglf (Δglf), and the double mutant lacking the CPS and the LPS O-polysaccharide, 52145- Δwca_{k2} -
1360 Δglf ($\Delta cps \Delta glf$) for 16 h. After 1 h contact, the medium was replaced with medium containing
1361 gentamicin (100 µg/ml) to kill extracellular bacteria.

1362 In panels C, D, and F images are representative of three independent experiments. In panels A, B,
1363 D, E, and G values are presented as the mean ± SD of three independent experiments measured in

1364 duplicate. **** $P \leq 0.0001$; ** $P \leq 0.01$; ns, $P > 0.05$ for the indicated comparisons determined
1365 using one way-ANOVA with Bonferroni contrast for multiple comparisons test.

1366 **Figure 5. *K. pneumoniae* induces SARM1 in a type I IFN-dependent manner.**

1367 A. *sarm1* mRNA levels were assessed by qPCR in wild-type macrophages (WT) non-infected (ni)
1368 or infected with Kp52145 for 16 h. After 1 h contact, the medium was replaced with medium
1369 containing gentamicin (100 $\mu\text{g/ml}$) to kill extracellular bacteria.

1370 B. *sarm1* mRNA levels were assessed by qPCR in the lungs of infected wild-type mice (WT) for 24
1371 h.

1372 C. Immunoblot analysis of SARM1-FLAG and tubulin levels in lysates of *Sarm1*^{FLAG} macrophages
1373 non-infected (NI) or infected with Kp52145 for the indicated time points. After 1 h contact, the
1374 medium was replaced with medium containing gentamicin (100 $\mu\text{g/ml}$) to kill extracellular bacteria.

1375 D. *sarm1* mRNA levels were assessed by qPCR in wild-type macrophages (WT), *myd88*^{-/-}, *ifnar1*^{-/-},
1376 *tlr4*^{-/-}, *tram*^{-/-}*trif*^{-/-}, and *irf3*^{-/-} non-infected (ni) or infected with Kp52145 for 6 and 16 h. After 1 h
1377 contact, the medium was replaced with medium containing gentamicin (100 $\mu\text{g/ml}$) to kill
1378 extracellular bacteria.

1379 E. *sarm1* mRNA levels were assessed by qPCR in wild-type macrophages (WT) non-infected (ni)
1380 or infected with Kp52145, the capsule mutant 52145- ΔmanC (Δcps), the mutant lacking the LPS O-
1381 polysaccharide, 52145- Δglf (Δglf), and the double mutant lacking the CPS and the LPS O-
1382 polysaccharide, 52145- Δwca_{k2} - Δglf (Δcps Δglf) for 16 h. After 1 h contact, the medium was
1383 replaced with medium containing gentamicin (100 $\mu\text{g/ml}$) to kill extracellular bacteria.

1384 In panel C, image is representative of three independent experiments. In panels A, B, D, and E
1385 values are presented as the mean \pm SD of three independent experiments measured in duplicate. In
1386 panels A, B and D **** $P \leq 0.0001$; *** $P \leq 0.001$; * $P \leq 0.05$ for the indicated comparisons; in panel
1387 C # $P \leq 0.0001$; ns, $P > 0.05$ for the comparisons between the knock-out and wild-type cells at the
1388 same time point post infection. Significance was established using one way-ANOVA with
1389 Bonferroni contrast for multiple comparisons test.

1390 **Figure 6. SARM1 is required for *K. pneumoniae* intracellular survival.**

1391 A. Kp52145 intracellular survival in wild-type (WT) and *sarm1*^{-/-} 4 h after addition of gentamycin
1392 (30 min of contact). Results are expressed as % of survival (CFUs at 4 h versus 1 h in *sarm1*^{-/-} cells
1393 normalized to the results obtained in wild-type macrophages set to 100%). Values are presented as
1394 the mean ± SD of six independent experiments measured in triplicate.

1395 B. Immunofluorescence confocal microscopy of the colocalization of Kp52145 harbouring
1396 pFPV25.1Cm and cresyl violet in wild-type (WT) and *sarm1*^{-/-} macrophages. The images were
1397 taken 90 min post infection. Images are representative of duplicate coverslips in three independent
1398 experiments.

1399 C. Percentage of Kp52145 harbouring pFPV25.1Cm co-localization with cresyl violet over a time
1400 course. Wild-type (WT) and *sarm1*^{-/-} macrophages were infected; coverslips were fixed and stained
1401 at the indicated times. Values are given as mean percentage of Kp52145 co-localizing with the
1402 marker ± SD. At least 200 infected cells belonging to three independent experiments were
1403 counted per time point.

1404 D. Immunoblot analysis of phosphorylated Akt (P-AKT), and tubulin levels in lysates of wild-type
1405 (WT) and *sarm1*^{-/-} macrophages non-infected (NI) or infected with Kp52145 for the indicated time
1406 points. After 1 h contact, the medium was replaced with medium containing gentamicin (100
1407 µg/ml) to kill extracellular bacteria. Images are representative of three independent experiments.

1408 E. Immunofluorescence confocal microscopy of the colocalization of Kp52145 harbouring
1409 pFPV25.1Cm, Lamp1, and Rab14 in wild-type (WT) and *sarm1*^{-/-} macrophages. The images were
1410 taken 90 min post infection. Images are representative of duplicate coverslips in three independent
1411 experiments.

1412 F. Percentage of Kp52145 harbouring pFPV25.1Cm co-localization with Lamp1 and Rab14 over a
1413 time course. Wild-type (WT) and *sarm1*^{-/-} macrophages were infected; coverslips were fixed and
1414 stained at the indicated times. Values are given as mean percentage of Kp52145 co-localizing with

1415 the marker \pm SD. The number of infected cells counted per time in three independent
1416 experiments are indicated in the figure.

1417 In panels, A, C and F, values are presented as the mean \pm SD of three independent experiments
1418 measured in duplicate. ****P \leq 0.0001; ***P \leq 0.001; ** P \leq 0.01; ns, P > 0.05 for the indicated
1419 comparisons determined using unpaired t test.

1420 **Figure 7. SARM1 promotes *K. pneumoniae* virulence.**

1421 A. *il1b*, *tnfa*, *il12*, *cxcl10*, *ifnb*, and *isg15* mRNA levels were assessed by qPCR in the lungs of
1422 infected wild-type mice (WT), *sarm1*^{-/-}, and *Sarm1*^{em1.1Tft} for 24. Each dot represents a different
1423 mouse.

1424 B. *il10* mRNA levels were assessed by qPCR in the lungs of infected wild-type (WT), *sarm1*^{-/-}, and
1425 *Sarm1*^{em1.1Tft} mice for 24.

1426 C. Percentage of immune cells in the lungs of wild-type (WT), and *sarm1*^{-/-} mice non-infected (ni)
1427 or infected intranasally with Kp52145 for 24. Results are based on data from three mice per group.

1428 D. PhenoGraph cluster analysis of immune populations in the lungs wild-type (WT), and *sarm1*^{-/-}
1429 mice non-infected (ni) or infected intranasally with Kp52145 for 24. Results are based on data from
1430 three mice per group.

1431 E. Heat map showing relative signal intensities of the indicated markers on neutrophils of clusters
1432 13, 15 found in the lungs of infected wild-type mice, and clusters 11 and 13 detected in the lungs of
1433 *sarm1*^{-/-} mice. The heat map is coloured based on signal intensity of the indicated markers. Results
1434 are based on data from three mice per group.

1435 F. Heat map showing relative signal intensities of the indicated markers on alveolar macrophages of
1436 clusters 5 and 6 found in the lungs of infected wild-type and *sarm1*^{-/-} mice. The heat map is
1437 coloured based on signal intensity of the indicated markers. Results are based on data from three
1438 mice per group.

1439 G. Heat map showing relative signal intensities of the indicated markers on interstitial macrophages
1440 of clusters 16 and 17 found in the lungs of infected wild-type and *sarm1*^{-/-} mice. The heat map is

1441 coloured based on signal intensity of the indicated markers. Results are based on data from three
1442 mice per group.

1443 H. Bacterial load in the lungs of infected wild-type mice (WT), *sarm1*^{-/-}, and *Sarm1*^{em1.1Tff} for 24.
1444 Each dot represents a different mouse.

1445 I. Bacterial load in the livers and spleens of infected wild-type mice (WT), *sarm1*^{-/-}, and
1446 *Sarm1*^{em1.1Tff} for 24. Each dot represents a different mouse.

1447 In panels A, B, H and I values are presented as the mean ± SD of three independent experiments
1448 measured in duplicate. ****P ≤ 0.0001; ***P ≤ 0.001; **P ≤ 0.01; *P ≤ 0.05; ns, P > 0.05 for the
1449 indicated comparisons using one way-ANOVA with Bonferroni contrast for multiple comparisons
1450 test.

1451 **Figure 8. *K. pneumoniae* exploits the immunomodulatory properties of SARM1 to antagonize**
1452 **cell intrinsic immunity.**

1453 Kp52145 activates the signalling pathway TLR4-TRAM-TRIF-IRF3 to induce the production of
1454 type I IFN, which signals through the IFNAR1 receptor (**). Type I IFN stimulates the
1455 transcription of SARM1, and AIM2 via IRF3. SARM1 negatively regulates MyD88 and TRIF-
1456 governed inflammatory responses, the activation of the MAP kinases ERK and JNK, and the AIM2
1457 inflammasome. In contrast, SARM1 is required for the activation of the MAP kinase p38, which
1458 controls the production of IL10. Kp52145 exploits IL10 to control inflammation. Absence of
1459 SARM1 impairs the intracellular survival of Kp52145, and *sarm1*^{-/-} mice do control Kp52145
1460 infection. Collectively, our findings illustrate the crucial role of SARM1 in *K. pneumoniae* immune
1461 evasion strategies.

1462

1463

1464

1465 **SUPPLEMENTARY FIGURE LEGENDS**

1466 **Figure S1. SARM1 negatively regulates *K. pneumoniae*-induced inflammation.**

1467 A. ELISA of TNF α , IL1 β , CXCL10 secreted by wild-type (WT) and *sarm1*^{-/-} BMDMs non-infected
1468 (ni) or infected with Kp52145 for 6 and 16 h. After 1 h contact, the medium was replaced with
1469 medium containing gentamicin (100 μ g/ml) to kill extracellular bacteria.

1470 B. Efficiency of transfection of SARM siRNA (siSARM) in wild-type iBMDMs. mRNA levels
1471 were assessed 16 h post transfection as fold change against control non-silencing agents AllStars
1472 (siAS).

1473 C. ELISA of IL1 β , TNF α , and CXCL10 secreted by wild-type (WT) macrophages transfected with
1474 All Stars siRNA control (siAS), or SARM1 siRNA (siSARM) non-infected (ni) or infected with
1475 Kp52145 for 16 h. After 1 h contact, the medium was replaced with medium containing gentamicin
1476 (100 μ g/ml) to kill extracellular bacteria.

1477 D. ELISA of IL1 β , TNF α , and CXCL10 secreted by wild-type (WT) and *Sarm1*^{em1.1Tjt} macrophages
1478 non-infected (ni) or infected with Kp52145 for 6 and 16 h. After 1 h contact, the medium was
1479 replaced with medium containing gentamicin (100 μ g/ml) to kill extracellular bacteria.

1480 In panels A, C, and D, values are presented as the mean \pm SD of three independent experiments
1481 measured in duplicate. ****P \leq 0.0001; **P \leq 0.01; *P \leq 0.05; for the indicated comparisons using
1482 one way-ANOVA with Bonferroni contrast for multiple comparisons test. In panel B, **P \leq 0.01
1483 using unpaired t test.

1484 **Figure S2. *K. pneumoniae* induction of IL10 is controlled by p38 and it is negatively regulated**
1485 **by type I IFN.**

1486 A. ELISA of IL10 secreted by wild-type macrophages non-infected (ni) or infected with Kp52145
1487 (Kp) 16 h. Cells were treated with the p38 inhibitor SB202190 or DMSO vehicle control. After 1 h
1488 contact, the medium was replaced with medium containing gentamicin (100 μ g/ml) to kill
1489 extracellular bacteria.

1490 B. Efficiency of transfection of SARM1 siRNA (siSARM) in *il10*^{-/-} macrophages. mRNA levels
1491 were assessed 16 h post transfection as fold change against control non-silencing agents AllStars
1492 (siAS).

1493 C. Immunoblot analysis of phosphorylated p38 (P-p38), and tubulin levels in lysates of wild-type
1494 (WT) and *ifnar1*^{-/-} macrophages non-infected (NI) or infected with Kp52145 for the indicated time
1495 points. After 1 h contact, the medium was replaced with medium containing gentamicin (100
1496 µg/ml) to kill extracellular bacteria.

1497 D. Immunoblot analysis of phosphorylated p38 (P-p38), and tubulin levels in lysates of wild-type
1498 (WT) and *tlr4*^{-/-} macrophages non-infected (NI) or infected with Kp52145 for the indicated time
1499 points. After 1 h contact, the medium was replaced with medium containing gentamicin (100
1500 µg/ml) to kill extracellular bacteria.

1501 E. Immunoblot analysis of phosphorylated p38 (P-p38), and tubulin levels in lysates of wild-type
1502 (WT) and *tram*^{-/-}*trif*^{-/-} macrophages non-infected (NI) or infected with Kp52145 for the indicated
1503 time points. After 1 h contact, the medium was replaced with medium containing gentamicin (100
1504 µg/ml) to kill extracellular bacteria.

1505 F. *il10* mRNA levels were assessed by qPCR, in wild-type (WT), *tlr4*^{-/-}, *tram*^{-/-}*trif*^{-/-}, and *ifnar1*^{-/-}
1506 macrophages non-infected (ni) or infected with Kp52145 for 6 and 16 h. After 1 h contact, the
1507 medium was replaced with medium containing gentamicin (100 µg/ml) to kill extracellular bacteria.

1508 In panel A, values are presented as the mean ± SD of three independent experiments measured in
1509 duplicate. ****P ≤ 0.0001 for the indicated comparisons using one way-ANOVA with Bonferroni
1510 contrast for multiple comparisons test. In panel B, values are presented as the mean ± SD of three
1511 independent experiments measured in duplicate. **P ≤ 0.01 using unpaired t test. In panel F, values
1512 are presented as the mean ± SD of three independent experiments measured in duplicate. ****P ≤
1513 0.0001 for the comparison between infected knock-out and wild-type cells for 6 h; # P ≤ 0.0001 for
1514 the comparison between infected knock-out and wild-type cells for 16 h using one way-ANOVA
1515 with Bonferroni contrast for multiple comparisons test.

1516 In panels C, D and E the images are representative of three independent experiments.

1517 **Figure S3. *K. pneumoniae* does not activate NLRP3 inflammasome.**

1518 A. ELISA of IL1 β secreted by wild-type (WT), *asc*^{-/-}, and *gsmd*^{-/-} macrophages non-infected (ni) or
1519 infected with Kp52145 (Kp) for 16 h. After 1 h contact, the medium was replaced with medium
1520 containing gentamicin (100 μ g/ml) to kill extracellular bacteria.

1521 B. Immunoblot analysis of processed pro-IL1 β , and β -actin levels in lysates of wild-type
1522 macrophages (WT) and *asc*^{-/-} and *gsmd*^{-/-} macrophages non-infected or infected with Kp52145 for
1523 16h. After 1 h contact, the medium was replaced with medium containing gentamicin (100 μ g/ml)
1524 to kill extracellular bacteria.

1525 C. ELISA of IL1 β secreted by wild-type (WT) macrophages non-infected (ni) or infected with
1526 Kp52145 (Kp) for 6 and 16 h. Cells were treated with the NLRP3 inhibitor MC950 or DMSO
1527 vehicle control. After 1 h contact, the medium was replaced with medium containing gentamicin
1528 (100 μ g/ml) to kill extracellular bacteria.

1529 D. ELISA of IL1 β secreted by wild-type (WT) and *nlrp3*^{-/-} macrophages non-infected (ni) or
1530 infected with Kp52145 for 6 and 16 h. After 1 h contact, the medium was replaced with medium
1531 containing gentamicin (100 μ g/ml) to kill extracellular bacteria.

1532 E. Immunoblot analysis of processed pro-IL1 β , and β -actin levels in lysates of wild-type
1533 macrophages (WT) and *nlrp3*^{-/-} macrophages non-infected or infected with Kp52145 for 16h. After
1534 1 h contact, the medium was replaced with medium containing gentamicin (100 μ g/ml) to kill
1535 extracellular bacteria.

1536 F. Immunoblot analysis of NLRP3 and tubulin levels in lysates of wild-type macrophages (WT) and
1537 *nlrp3*^{-/-} macrophages non-infected (NI) or infected with Kp52145 for the indicated time points.
1538 After 1 h contact, the medium was replaced with medium containing gentamicin (100 μ g/ml) to kill
1539 extracellular bacteria.

1540 G. Efficiency of transfection of AIM2 siRNA (siAIM2) in *sarm1*^{-/-} macrophages. mRNA levels
1541 were assessed 16 h post transfection as fold change against control non-silencing agents AllStars
1542 (siAS).

1543 In panels A, C and D values are presented as the mean \pm SD of three independent experiments
1544 measured in duplicate. **** $P \leq 0.0001$; ns, $P > 0.05$ for the indicated comparisons using one way-
1545 ANOVA with Bonferroni contrast for multiple comparisons test. In panel G, values are presented as
1546 the mean \pm SD of three independent experiments measured in duplicate. ** $P \leq 0.01$ using unpaired t
1547 test. In panels B, E and F, images are representative of three independent experiments.

1548 **Figure S4. *K. pneumoniae* induction of AIM2 is TLR4-TRAM-TRIF-IRF3 dependent.**

1549 A. *aim2* mRNA levels were assessed by qPCR, in wild-type (WT), *myd88*^{-/-}, *tlr4*^{-/-}, *tram*^{-/-}*trif*^{-/-}, and
1550 *irf3*^{-/-} macrophages non-infected (ni) or infected with Kp52145 for 6 and 16 h. After 1 h contact,
1551 the medium was replaced with medium containing gentamicin (100 μ g/ml) to kill extracellular
1552 bacteria.

1553 B. Immunoblot analysis of AIM2 and β -actin levels in lysates of wild-type (WT), *tlr4*^{-/-} and *tram*^{-/-}
1554 *trif*^{-/-} macrophages non-infected (NI) or infected with Kp52145 for the indicated time points. After 1
1555 h contact, the medium was replaced with medium containing gentamicin (100 μ g/ml) to kill
1556 extracellular bacteria.

1557 C. ELISA of IL1 β secreted by wild-type (WT), *tlr4*^{-/-}, *tram*^{-/-}*trif*^{-/-} and *ifnar1*^{-/-} macrophages non-
1558 infected (ni) or infected with Kp52145 for 6 and 16 h. After 1 h contact, the medium was replaced
1559 with medium containing gentamicin (100 μ g/ml) to kill extracellular bacteria.

1560 D. Immunoblot analysis of pro-IL1 β and β -actin levels in lysates of wild-type (WT), and *tlr4*^{-/-}
1561 macrophages non-infected (NI) or infected with Kp52145 for the indicated time points. After 1 h
1562 contact, the medium was replaced with medium containing gentamicin (100 μ g/ml) to kill
1563 extracellular bacteria.

1564 In panels A and C, values are presented as the mean \pm SD of three independent experiments
1565 measured in duplicate. # $P \leq 0.0001$; ns, $P > 0.05$ for the comparison between knockout and wild-
1566 type cells at 6 or 16 h post infection using one way-ANOVA with Bonferroni contrast for multiple
1567 comparisons test. In panels B and D, images are representative of three independent experiments.

1568 **Figure S5. Adhesion and phagocytosis of *K. pneumoniae* by *sarm1*^{-/-} macrophages.**

1569 A. Adhesion in wild-type (WT) and *sarm1*^{-/-} macrophages. Cells were infected with Kp52145 for 30
1570 min, wells were washed and bacteria were quantified by lysis, serial dilution and viable counting on
1571 LB agar plates.

1572 B. Phagocytosis of Kp52145 by wild-type (WT) and *sarm1*^{-/-} macrophages. Cells were infected for
1573 30 min, wells were washed, and it was added medium containing gentamicin (100 µg/ml) to kill
1574 extracellular bacteria. After 30 min, cells were washed and bacteria were quantified by lysis, serial
1575 dilution and viable counting on LB agar plates.

1576 In panels A and B, values are presented as the mean ± SD of three independent experiments
1577 measured in triplicate. * P ≤ 0.05; ns, P > 0.05 for the indicated comparisons using unpaired t test.

1578 **Figure S6. Description of mouse immune populations following *K. pneumoniae* infection.**

1579 A. PhenoGraph cluster analysis of immune populations in the lungs wild-type (WT), and *sarm1*^{-/-}
1580 mice non-infected (ni) or infected intranasally with Kp52145 for 24. Graphs shows the combine
1581 results of all groups.

1582 B. Heat map showing relative signal intensities of the indicated markers on the clusters identified in
1583 panel A. The heat map is coloured based on signal intensity of the indicated markers. Results are
1584 based on data from three mice per group.

1585 C. PhenoGraph cluster analysis of immune populations in the lungs wild-type (WT), and *sarm1*^{-/-}
1586 mice non-infected (ni) or infected intranasally with Kp52145 for 24. Each graph represents an
1587 individual mouse.

1588

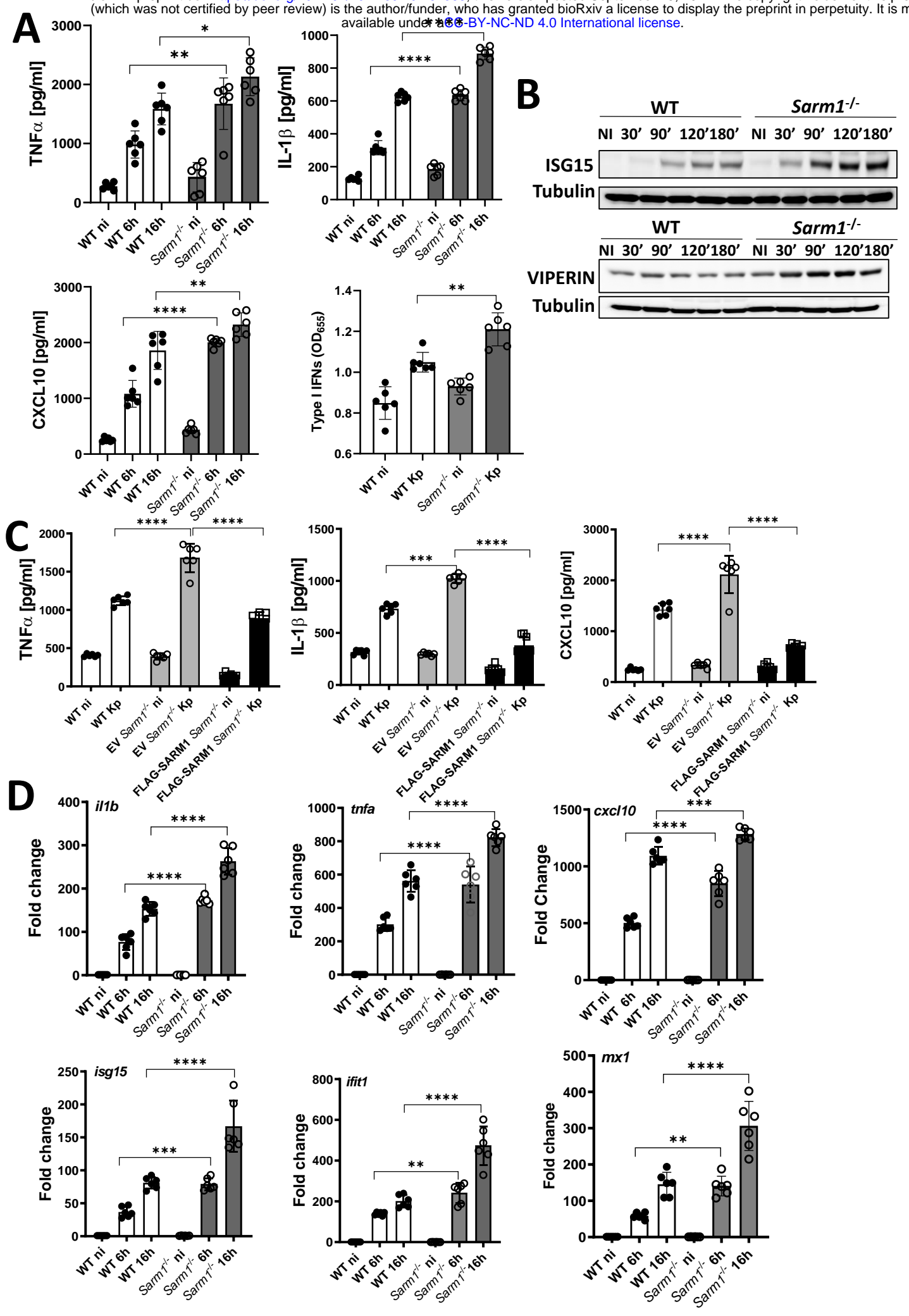
1589

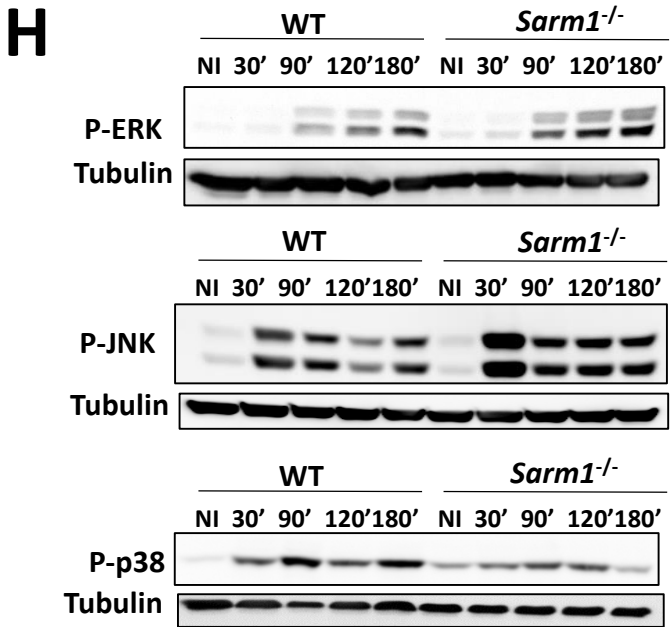
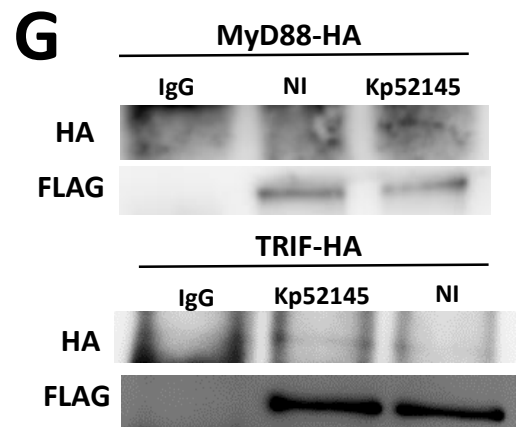
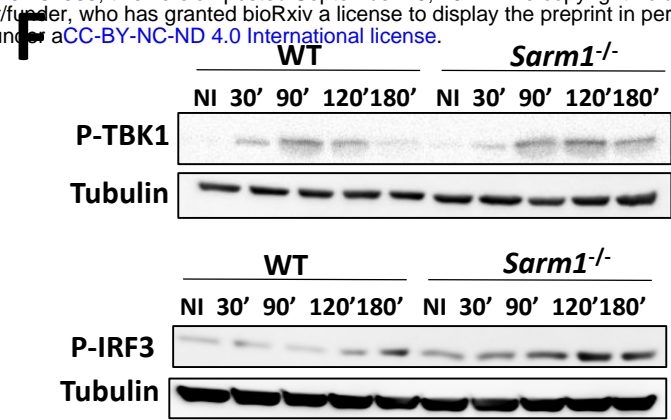
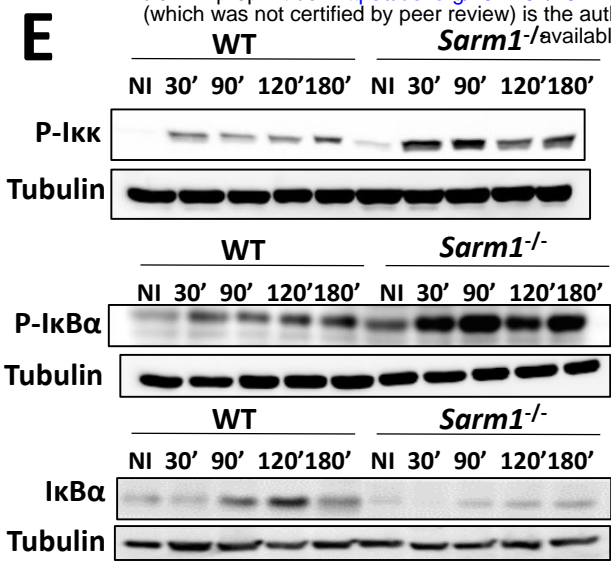
1590

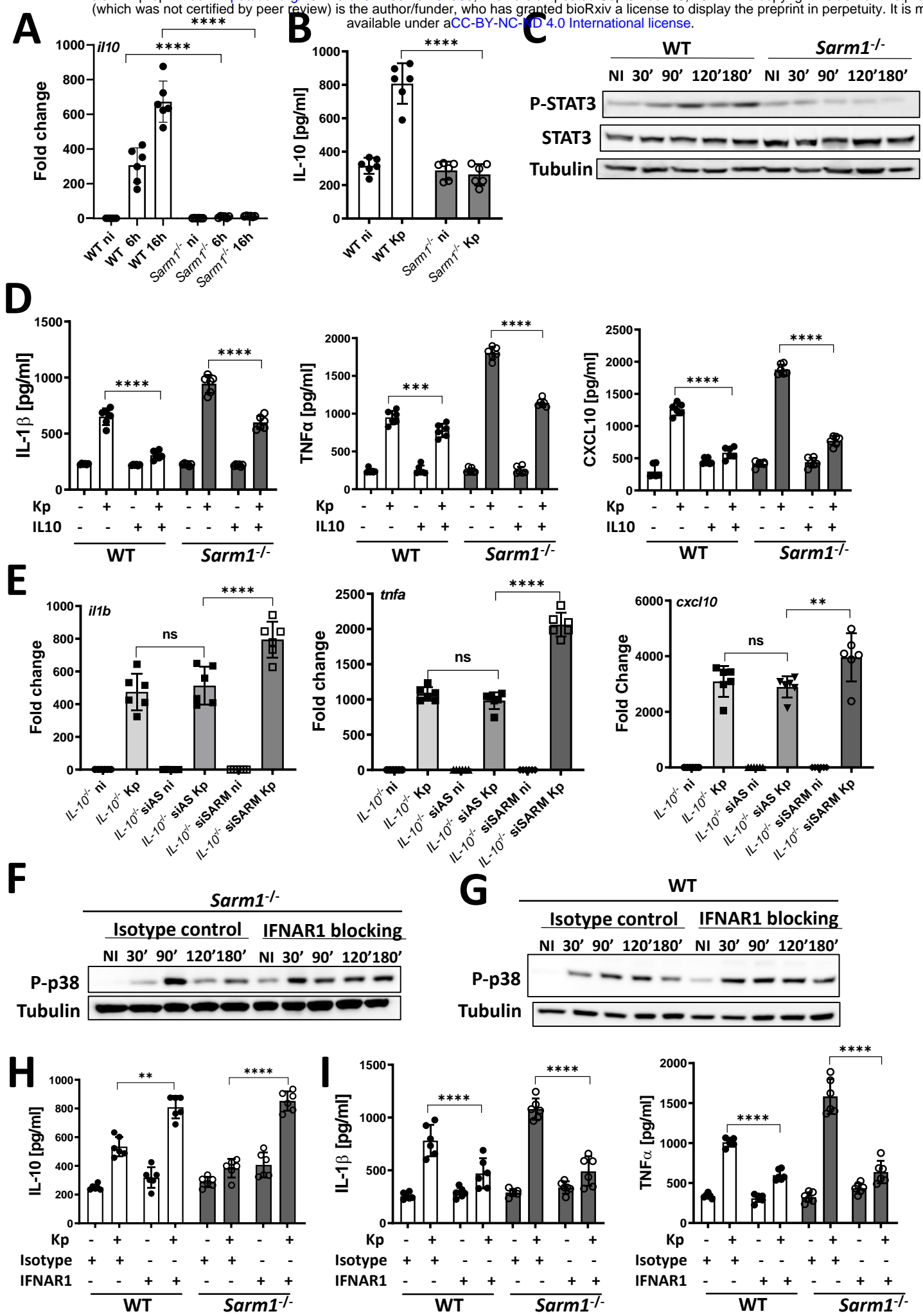
1591

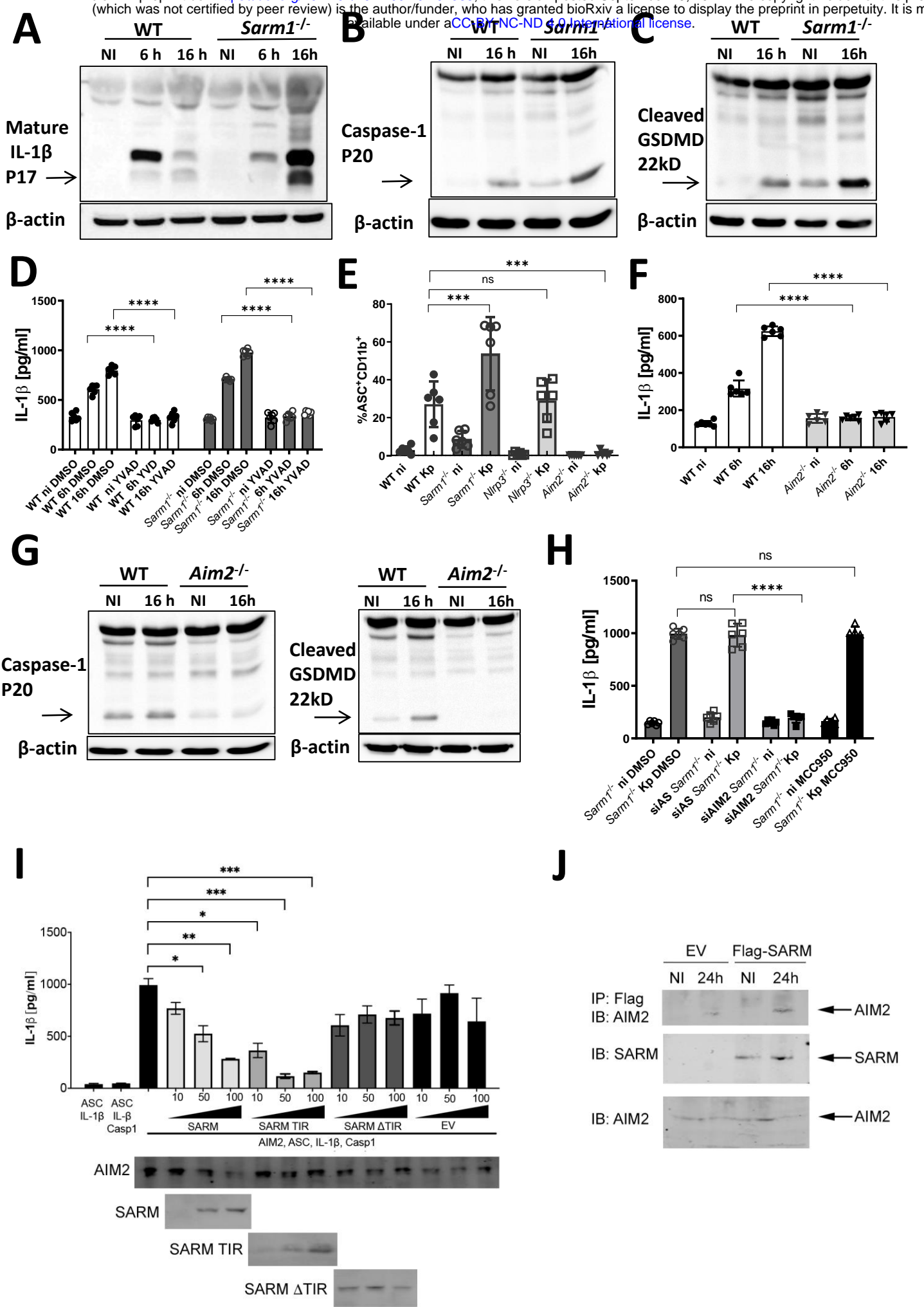
1592

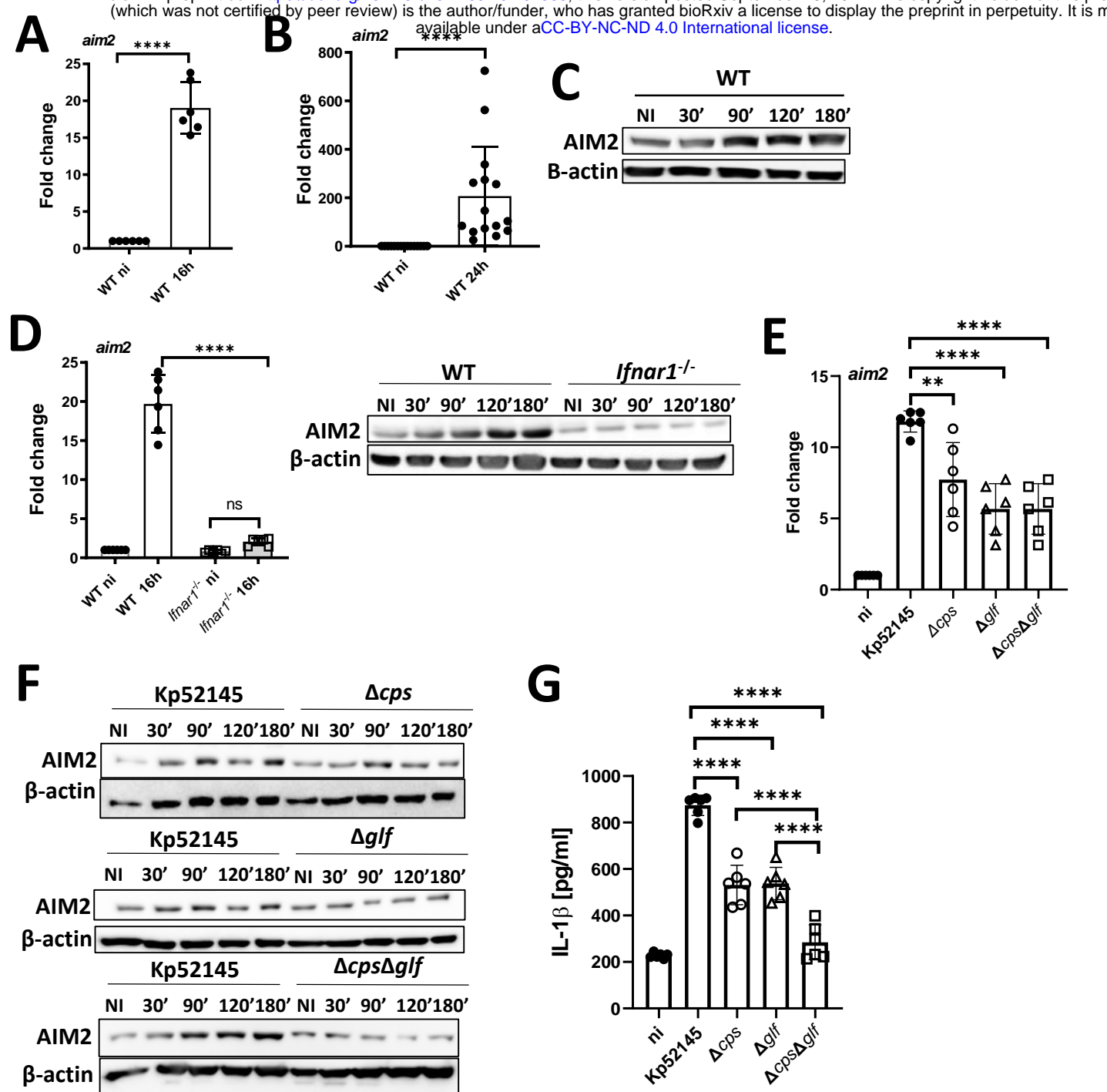
1593

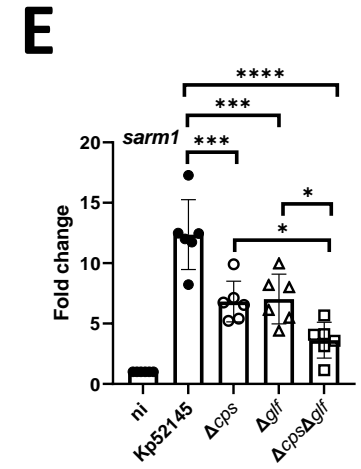
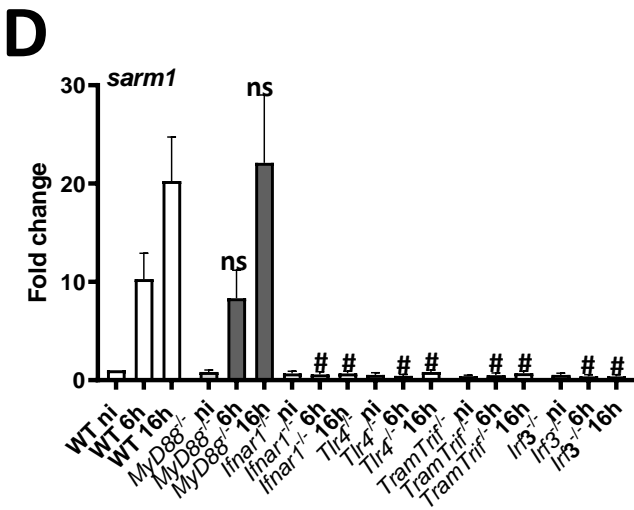
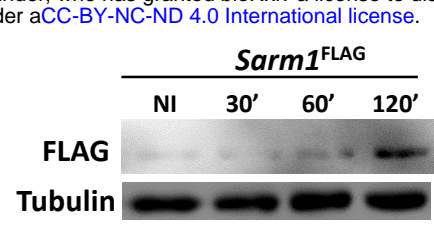
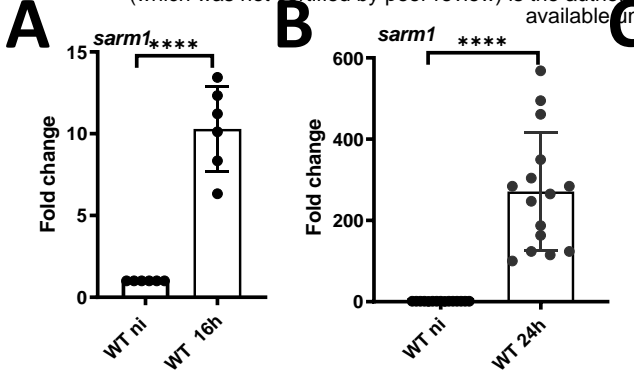


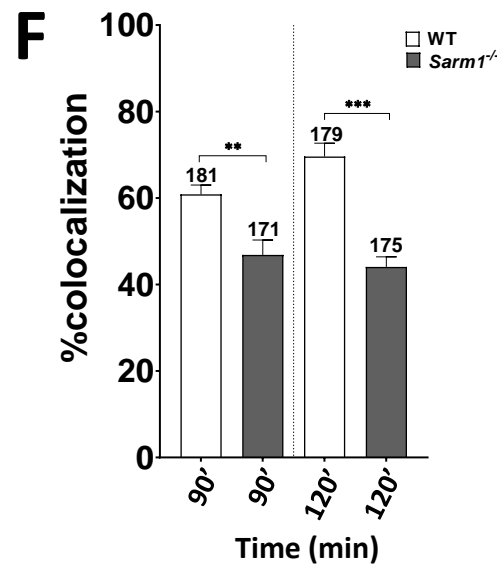
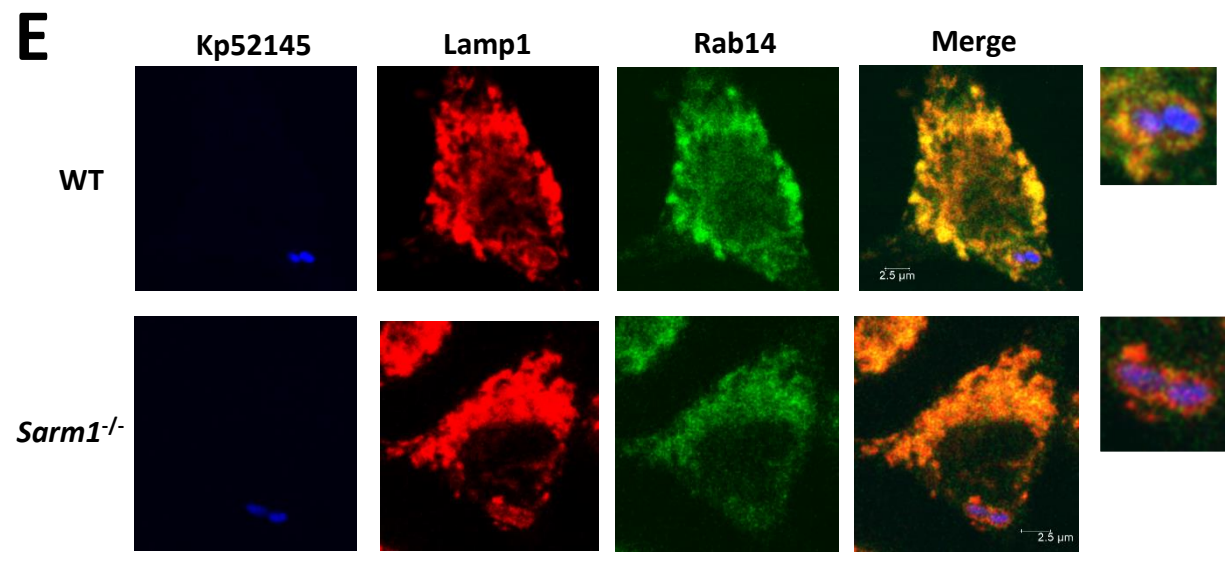
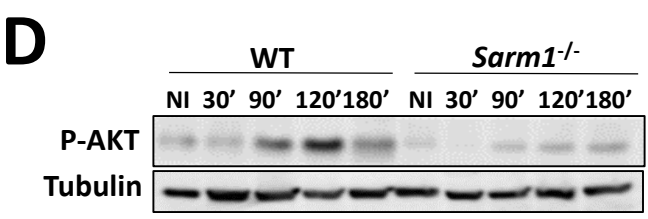
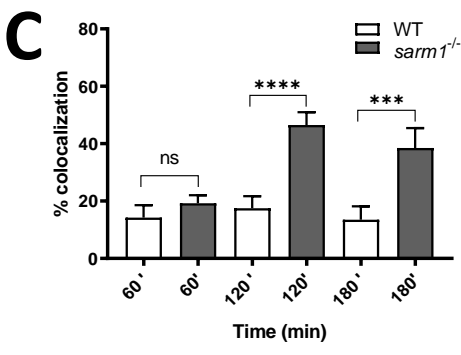
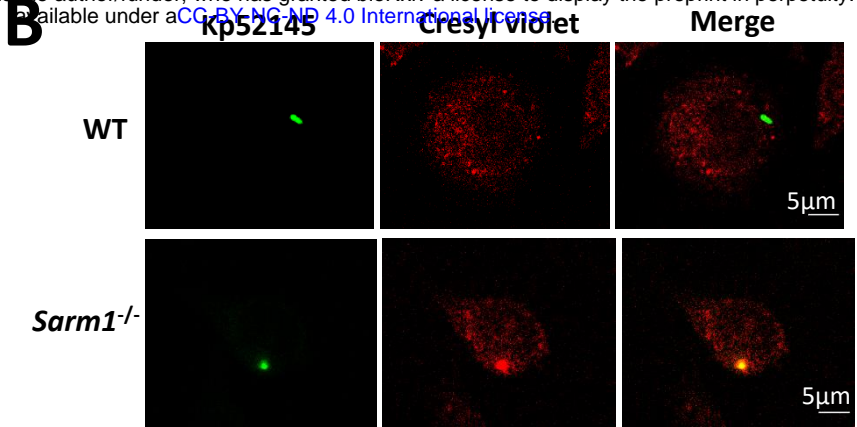
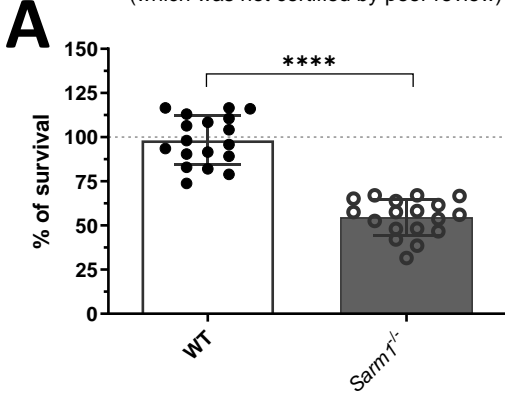




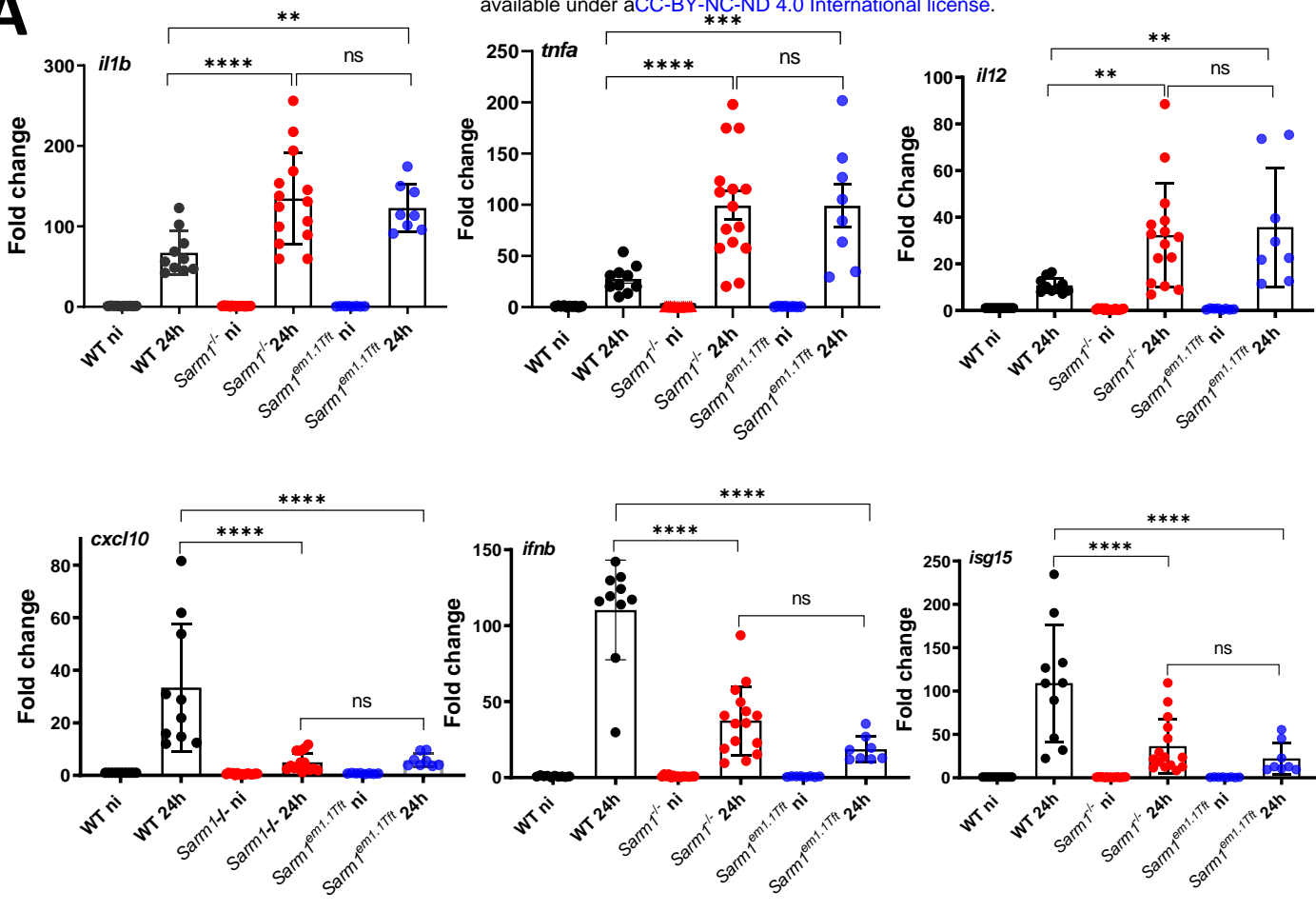




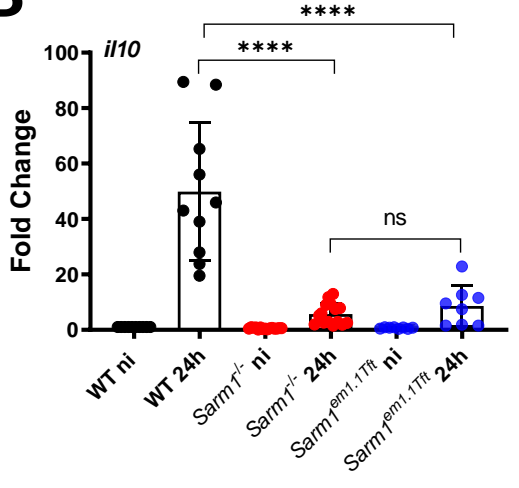




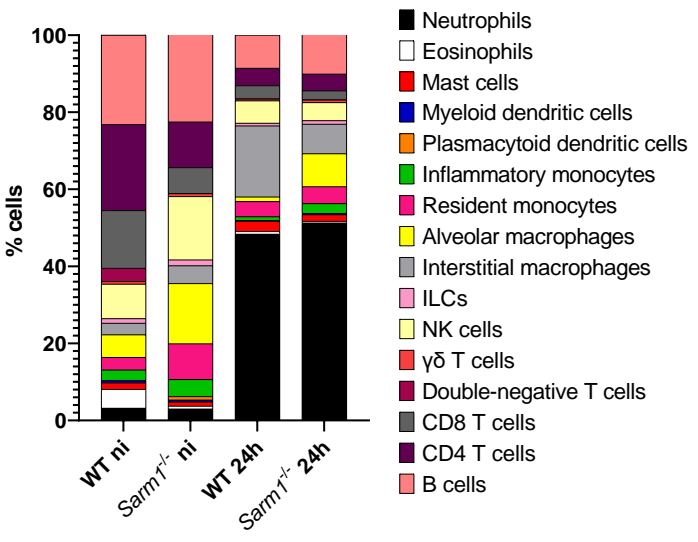
A



B



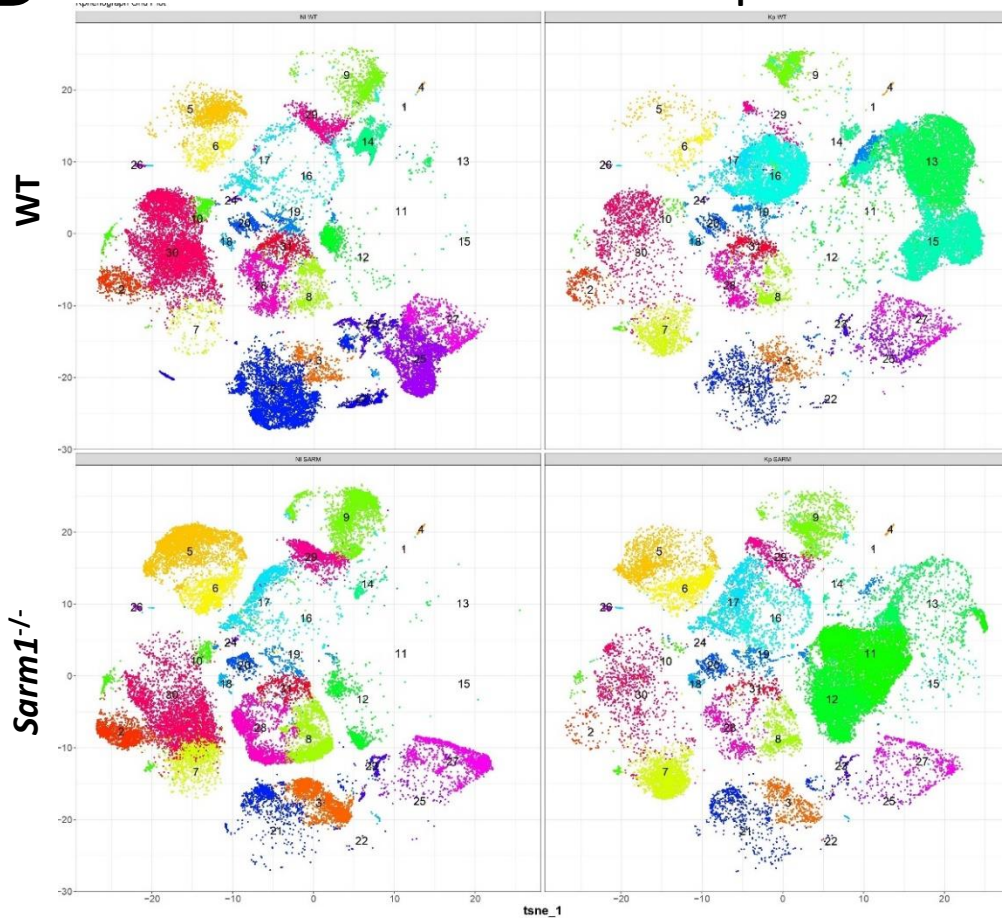
C



D

ni

Kp52145



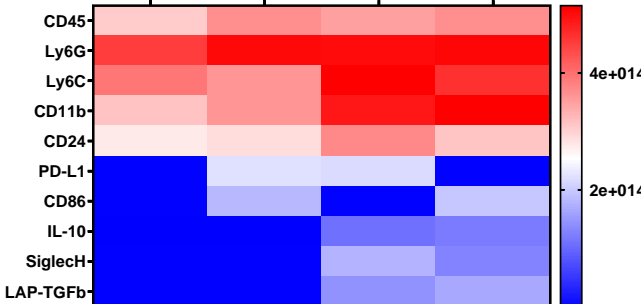
E

Neutrophils

WT

***Sarm1*^{-/-}**

CLUSTER 13 CLUSTER 15 CLUSTER 11 CLUSTER 12

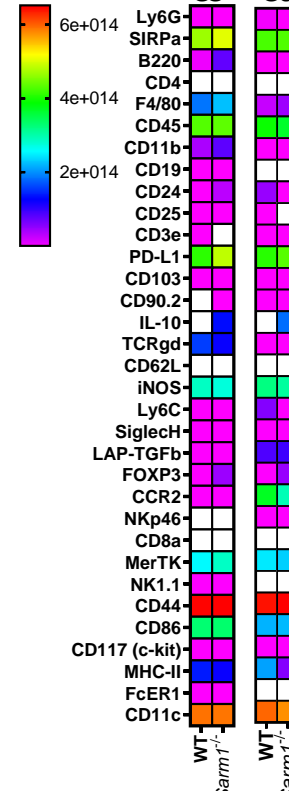


F

Alveolar macrophages

C5

C6

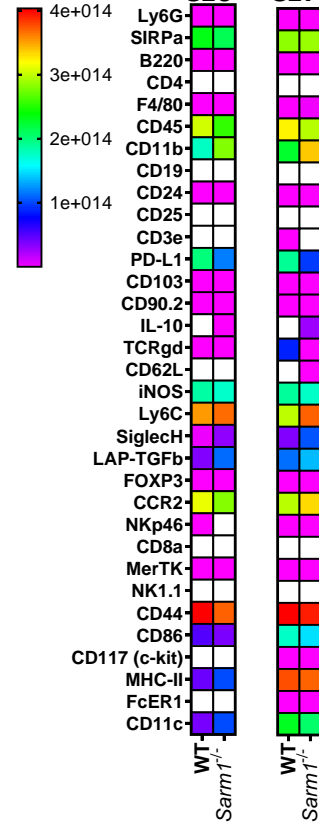


G

Interstitial macrophages

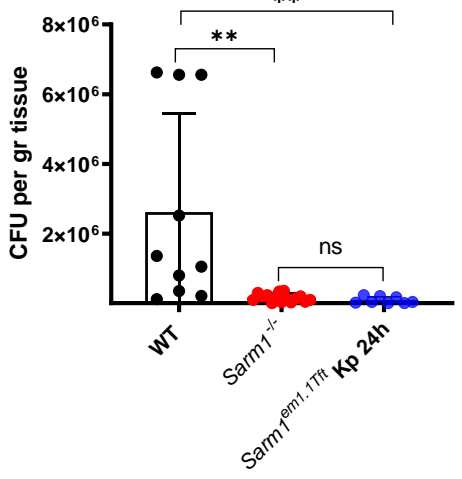
C16

C17

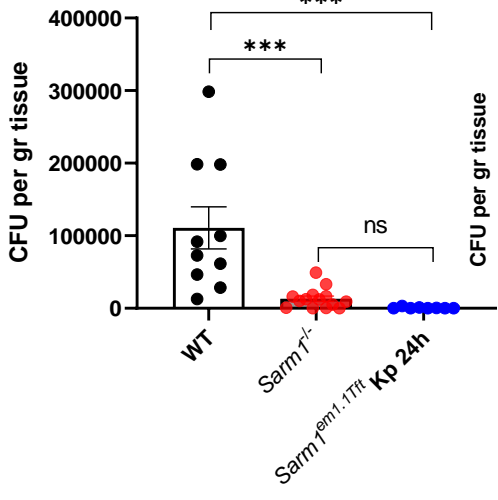


H

Lung



Liver



Spleen

